7-6-2022

# MICRO HEAT EXCHANGER TO COOL CEREBROSPINAL FLUID FOR BRAIN INJURY TREATMENT

Sachin Dahiya
*Louisiana State University and Agricultural and Mechanical College*

# MICRO HEAT EXCHANGER TO COOL CEREBROSPINAL FLUID FOR BRAIN INJURY TREATMENT

A Thesis

Submitted to the Graduate Faculty of the
Louisiana State University and
Agricultural and Mechanical College
in partial fulfilment of the
requirements for the degree of
Master of Science

in

The Department of Mechanical and Industrial Engineering

by
Sachin Dahiya
B.Tech., Maharishi Markandeshwar University, 2019
August 2022

## Acknowledgments

Foremost, I would like to acknowledge and thank my supervisor Dr. Manas Ranjan Gartia, without whom this work could not have been possible. His motivation and guidance inspired me to work hard and tackle any obstacles that I encountered at the time of research and writing of this thesis. My mother, Ms. Poonam, and my sister Ms. Shalini also played a vital role in encouraging me to study overseas and providing continuous support when needed. I would furthermore like to thank my colleague Mr. Mohana Gurunandhan for pointing me in the right direction during various phases of this work.

Other than my supervisor, peer, and family, I would like to extend my sincere gratitude to the rest of my committee members, Dr. Ram Devireddy, and Dr. Corina Barbalata, for being a part of this work. I am grateful to Dr. Devireddy for giving me an opportunity to work as a teaching assistant for thermal systems lab throughout my study period. I would also like to thank Dr. Daniel Park for his valuable contribution to this work and for assisting me on several occasions whenever I required him. Moreover, my friend Mr. Kaushik Sunder had a significant character in encouraging me to complete my thesis.

Finally, I would like to credit all the faculty and maintenance staff at Patrick F. Taylor Hall for ensuring that we have a safe and clean environment to work with during these unprecedented times.

# Table of Contents

# Nomenclature

| **General Symbols** | | | | | |
|---|---|---|---|---|---|
| $\bar{V}$ | Velocity vector | $[\frac{m}{s}]$ | $W_y$ | Depth of the channel | [mm] |
| $C_p$ | Specific heat | $[\frac{J}{kg*K}]$ | x,y,z | Width, depth, length | [mm] |
| a | Temperature | [K] | **Greek Symbols** | | |
| K | Thermal conductivity | $[\frac{W}{m*K}]$ | ρ | Density of fluid | $[\frac{kg}{m^3}]$ |
| V | Velocity | $[\frac{m}{s}]$ | ∇P | Pressure drop | [Pa] |
| $D_h$ | Hydraulic diameter | [mm] | μ | Dynamic viscosity | $[\frac{kg}{m*s}]$ |
| Re | Reynolds number | | ∇a | Temperature difference | [K] |
| Nu | Nusselt number | | **Subscripts and Superscripts** | | |
| Pr | Prandtl number | | i | Channel | |
| h | Heat transfer coefficient | $[\frac{W}{m^2*K}]$ | j | Fin | |
| u | Flow velocity | $[\frac{m}{s}]$ | l | Liquid | |
| q'' | Heat flux | $[\frac{W}{m^2}]$ | s | Solid | |
| $W_x$ | Width of the channel | [mm] | * | Non-dimensional variable | |
| $W_z$ | Length of the channel | [mm] | 1 | Inlet | |
| $W_{xj}$ | Width of solid fin | [mm] | 2 | Outlet | |
| n | Number of microchannels | | – | Average of the function | |
| $\dot{m}$ | Mass flow rate | $[\frac{kg}{s}]$ | | | |

## Abstract

Hypothermia is accepted as a method to preserve cells and tissue. Clinical evidence shows that administration of hypothermia could lead to neuroprotection after cardiac arrest. Non-invasive methods such as surface cooling devices, drugs and cold liquid ventilation are available to induce hypothermia. These approaches for achieving hypothermia have not been optimized yet. The surface cooling methods are generally slow and may lead to additional thermal shock to the body. Here, we propose a rapid, selective cooling method for the brain using a micro heat exchanger to cool the cerebrospinal fluids (CSF). We designed and 3D printed a U-type heat exchanger utilizing UV resin as the material for the heat exchanger as it has good mechanical and thermal properties. The heat exchanger has the inlet and outlet at the centre on both ends. There are seven channels for fluid flow and eight fins around the channels. The heat exchanger is placed on a Peltier component to keep the temperature constant across the heat exchanger. A syringe filled with CSF was utilized, which was placed on a syringe pump to provide the fluid at the inlet through the tube connections. To test the heat exchanger's efficiency, an artificial CSF was allowed to flow through it, and the surface and the outlet temperature were captured. Various parameters were optimized, such as the flow rate, the initial CSF temperature at the inlet, the voltage to be supplied to run the Peltier. This report presents theoretical and experimental results for Micro Heat Exchanger. Fluid flow behavior was investigated analytically as well as using a CFD code (ANSYS Fluent). The theoretical results were validated with the experimental results by measuring the surface and fluid temperature of the heat exchanger at specific locations. Overall, we saw a close agreement between the simulated and experimental results for the surface and outlet temperature. The U-type heat exchanger micromodel will improve the understanding of complex flow patterns in 3D and open a new approach for treating brain injuries in humans and animals with small form factors.

# Chapter 1. Introduction

## 1.1. Why is Cerebrospinal Fluid (CSF) analysis critical in Brain Injury Treatment?

A variety of substances, including glucose, protein, and white blood cells, enter the brain with the help of a primary route provided by the CSF system. A CSF study can be used to identify various medical conditions that affect the Central Nervous System (CNS). CSF investigation can precisely diagnose diseases that are difficult to detect otherwise, such as meningitis, tumour in the brain, multiple sclerosis, etc. CSF analysis is a collection of tests that examine a living being's CSF concentration to aid in the diagnosis of diseases affecting the brain. To perform a CSF analysis, a sample of CSF is required. The usual approach to obtaining this sample is through a lumbar puncture, often known as a spinal tap. Cisternal puncture, Ventricular puncture, and other less frequent methods of obtaining a fluid sample are among the less common techniques.

Before being taken into the bloodstream, CSF circulates throughout the brain's inner ventricle system. When the brain is jolted, CSF protects the brain tissue. CSF acts as a protective fluid for the brain, protecting it from mechanical harm and lowering the effective weight of the brain. The brain can be considered a water-cooled system with CSF as a heat-removal medium. When there are difficulties with CSF flow, CSF movement and blood flow might get affected, making neurons vulnerable. Cerebral blood flow may be impeded when CSF pressure is high. Many disorders, including Alzheimer's disease, ischemia, and neuroinflammatory syndromes, are thought to be caused by normal CSF circulation and turnover disruption. According to recent insights into CSF biology, CSF circulation may interact closely with glial and vascular functions to regulate basic elements of brain function [1]. The surface area of interaction between the CSF and the brain is enormous. CSF's massive fluid-brain contact surface is critical for the CNS's metabolic and thermal environment to stabilise and finely regulate.

### 1.1.1. Cerebrospinal Fluid (CSF)

The cerebrospinal fluid (CSF) is a transparent, watery fluid surrounding and protecting the brain and spinal cord. The choroid plexus tissue of the brain's ventricles produces CSF. CSF is created at a rate of about 500 millilitres each day, with approximately 150 millilitres in the body at any given time [2]. The amount of CSF secreted varies from person to person, although it ranges typically between 400 and 600 millilitres each day in adults. CSF is continuously created, ensuring that the fluid circulates around the central nervous system. The fluid will travel from the lateral ventricle to the third and fourth ventricles. Through the medial foramen of Magendie, fluid from the fourth ventricle travels to the subarachnoid space and the central canal of the spinal cord [3].

CSF has five main functions: buoyancy, protection, chemical stability, waste elimination, and brain ischemia prevention [4]. The brain weighs about 1400g, yet it only has a net weight of 50g due to the presence of CSF, which creates a bath [5]. Blood arteries and nerve roots, both of which are delicate structures, support the brain within the arachnoid space. CSF works as a shock absorber, protecting the brain from harm when it collides with the skull. It also maintains the external environment by regulating the transport of metabolites around the brain. The waste products of the brain cells are excreted into the CSF, which eventually drains into the bloodstream.

### 1.1.2. Traumatic Brain Injury (TBI)

TBI is a leading cause of adult disability and death around the world [6]. A TBI is a brain injury that occurs when a sudden trauma causes damage to the brain. A brain injury can be severe, from a minor concussion to a severe injury resulting in coma or death. Following the initial trauma, various secondary injury processes might occur, potentially leading to degeneration and irreparable brain damage. A TBI can affect anyone, although men are responsible for nearly 80% of all TBIs [7]. Adults over the age of 65 are more likely to suffer from

TBIs. This age group is more likely to lose their balance, fall, and strike their heads. It's still unknown how degenerative brain disorders and brain traumas are linked. However, some researchers suggest that traumatic brain injuries may raise the risk of degenerative brain illnesses, especially repetitive or severe ones. TBIs that are mild to moderate may simply require modest therapy. People with severe TBI often require hospitalization and more intensive treatment.

#### 1.1.3. Non-Traumatic Brain Injury (NTBI)

NTBI is a brain injury not caused by an external physical force to the head, such as a lack of oxygen or tumour pressure. NTBI can be caused by a stroke, a brain tumour, an infection, poisoning, or drug addiction [8]. Cells all around the brain are affected by NTBI. Because it disrupts the cellular structure, non-traumatic brain injury can spread throughout the brain. NTBIs can damage a person's physical, cognitive, emotional, and behavioural well-being and can happen at any age. However, it is crucial to note that brain injuries caused by non-traumatic causes can have harmful and long-term implications.

### 1.2. Current approaches in Brain Cooling

#### 1.2.1. Selective Brain Cooling Methods

Therapeutic hypothermia (TH) is a clinically established neuroprotective therapy accessible today. Although it appears that targeting lower temperatures during TH benefits ischemic brain cells, the systemic side effects associated with global hypothermia restrict its therapeutic utility. As a result, the ability to reduce brain temperature selectively while minimizing core temperature has the potential to maximize neurological benefits while minimizing systemic problems. In this circumstance, selective brain cooling (SBC) has emerged as a viable TH technique. The selective brain cooling (SBC) process keeps the brain colder than the rest of the body. The internal carotid artery is anatomically close to the cavernous sinus hence cooling the nasal cavities lowers brain temperature. In one study, the RhinoChill de-

vice was utilized to test the feasibility of intranasal evaporative cooling [9]. The RhinoChill device uses a catheter system to evaporate perfluorocarbon and oxygen at a 40–60 L/min flow rate into the nasal cavity, resulting in rapid hypothermia induction. However, because preventing brain injury may necessitate up to 12–24 hours of continuous brain cooling, the expense of RhinoChill will be excessive. In terms of cooling technologies' success in lowering brain temperature, selective brain cooling performs significantly better than other ways of obtaining the desired temperature. In homeotherms, there are two types of SBC: (1) cold venous blood returns from the nose and head skin, precooling arterial blood heading for the brain, and (2) cooling the brain directly with venous blood. SBC intensity is controlled via a single process. Reduced sympathetic activity causes the angular oculi veins, which supply the cerebral heat exchangers, to dilate while the facial veins, which supply the heart, contract. As a result, SBC increases during heat exposure, endurance exercise, relaxed wakefulness, and NREM sleep while decreasing during cold exposure and uncomfortable emotions. SBC is a multifunctional effector mechanism that helps to prolong exhaustion in athletic animals and protects the brain from heat injury. It also increases in dehydrated mammals to conserve water and may thermally control alertness. In order to improve diving ability and protect the brain from suffocation, it is also employed in diving animals to reduce cerebral temperature well below normal ranges. SBC combines both thermal and non-thermal regulation functions in one package. Selective brain cooling has been observed in several animal species; however, no studies have shown that humans are capable of selective brain cooling; the human airway is too short and too disconnected from the arterial blood that supplies the brain to allow air temperature to have a significant impact on brain temperature.

1.2.2. Thermo-Radiating Brain Cooling (TRBC)

Most brain cooling procedures currently use whole-body cooling; however, lowering the whole-body temperature below 34 °C might cause serious difficulties [10]. Thermo-

Radiating Brain Cooling (TRBC) cooling induction was used by Dohi and colleagues: A 16 fg Foley "balloon" catheter was used to administer 8–12 l/min of chilled (24 °C) air via one nostril while blocking the other with an epistaxis balloon. The air was then discharged through the mouth [11]. It's not entirely apparent, but it appears like the Foley catheter balloon was inflated to prevent air from seeping back out of the nostril, potentially reducing heat loss and contributing to nasal erosion. It is emphasized the need of allowing air to escape from the mouth. In individuals with global cerebral ischemia, such as cardiac arrest patients and new-borns with hypoxic-ischemic encephalopathy, hypothermia improves neurologic prognosis and reduces mortality. If two conditions are satisfied, a sufficiently low cerebral blood flow and a suitably high heat transfer coefficient, which describes the heat exchange between the head surface and the airflow rate, TRBC can successfully induce moderate hypothermia. The first criterion defines a requirement for using cooling devices to achieve mild hypothermia therapy. The cooling equipment must meet technical standards in the second criterion. However, this cooling method has some drawbacks, including insufficient cooling and irritating effects on skin contact areas.

### 1.2.3. Direct Brain Cooling

Numerous studies show that targeted brain cooling is an effective treatment option for people with severe traumatic brain damage [11, 12]. Targeted brain cooling is an excellent option to systemic hypothermia since it has fewer negative effects on the circulatory system, infection risk, electrolyte balance, and coagulopathy. Central venous catheters are used in internal cooling techniques to either provide ice-cold saline or to reduce blood temperature directly by convection. Instrumentation systems can be incorporated on a chip-level, allowing the system to be miniaturised to micro dimensions, thanks to advancements in the microelectronic sector. The miniaturisation of microcontrollers, which makes it easier to interface with sensing instrumentation systems, is one of the advancements. Using Programmable System

on Chip (PSoC), Idris and his team proposed a simple and clever localised brain cooling probe [12]. This system benefits from being straightforward, localising cooling areas in the brain, and being a System on Chip (SoC) based automation system. It entails creating a temperature chamber where sterile fluid connected to antibiotic pipework is delivered directly to the brain. The temperature controller will be inserted into the chamber, which the PSoC microcontroller will then process. The system will then be interfaced with the sensing and microcontroller for temperature display. D-Brain Cooling Machine is the name of this direct brain cooling machine. Although direct brain cooling therapy appears to be a potential treatment for severe head injuries, Idris is currently conducting a trial in severely head wounded patients utilising this newly created cooling machine [12]. As a result, this technology, which has one of its key goals as the development of direct targeted brain cooling, is still in the early stages of development and will require some time before it can be used in the actual world.

1.2.4. Non-Invasive Cooling

Even if cooling therapies are further typically provided structurally, the idea supporting head cooling is that it delivers cooling where needed since cerebral protection is more dependent on brain temperature than on trunk temperature. While any evidence does not support this proof, it is assumed that head cooling may lessen hypothermia problems by requiring less body temperature lowering.

No matter how it is delivered, cooling must lower brain temperature in order to have a neuroprotective impact. The key criterion for assessing the usefulness of head cooling in terms of temperature depletion is a drop in intracranial temperature. The temperature of the dura and inside the skull is known as intracranial temperature. The curtailment in core temperature respect to head cooling, which is detected in an artery (typically pulmonary), the oesophagus, the bladder, or the rectum, serves as a backup measure in the absence of data on

intracranial temperature. This is based on the presumption that if core temperature decreased, intracranial temperature must have followed suit.

Non-invasive cooling technologies are often rapid and straightforward to use. They might be suited for pre-hospital work, which are vital factors to consider when lowering cooling time if neuroprotection is the goal. They could also have a broad range of applications because they can be utilized in individuals with a variety of illnesses, not simply the most seriously afflicted [13]. The temperature of the brain will be assessed non-invasively in this manner.

There are two types of non-invasive head cooling methods. The first technique involves heat loss by convection from the top airways created by gas/fluid movement and conduction created by pharyngeal/nasal balloons. The second approach is convection, which involves distributing cool water/air and/or by conduction, which can be active or passive [14]. Some of the gadgets also have a neck band that, in theory, might aid in brain cooling by lowering the temperature of the carotid blood supply.

Cooling helmets that circulate water with or without antifreeze are known as liquid (active) cooling helmets. Conduction transfers heat from the head to the helmet wall, which is then removed by the circulating coolant. These cooling helmets can keep a steady temperature, and some even can alter the temperature. This is possibly crucial since lowering the scalp temperature to a greater extent can cause tissue freezing and necrosis. Compliant (non-circulating) heat reduction caps, such as those utilizing chilled gel, may thaw and need to be refrozen on a regular basis, although they are easy and inexpensive. Ice packs around the head are the cheapest approach. For optimal heat evacuation, the helmet or cap must be in close contact with the scalp, whether it is active or passive, which may necessitate pressurization.

Heat is lost as it moves through temperature rise from hot to cold. Convective heat reduction systems employ airflow or gas flow to eliminate heat; as molecules are withdrawn in large quantities, heat is transferred in the operation. Convective processes also permit for evaporation, a sort of convection whereby water loss mediates the bulk movement of molecules (converting water to water vapour requires huge quantities of heat). While molecules do not move over conductive paths, energy (heat) does. The device's wall transfers heat from the head, which is calmly pre-occupied by the frozen substance (gel or ice) or actively evacuated by the liquid coolant circulating inside. In this process, gadgets carrying chilled substance heats up and desired to be substituted on a frequent basis to maintain cooling efficiency.

The fact that the reduction in the temperature of the brain may be slightly impacted by body mass compared to the fall in core temperature is one potential benefit of head cooling. The implication is that non-invasive head cooling can significantly lower brain temperature within a short period of time. Despite being non-invasive, these treatments can have certain disadvantages, such as difficult application, particularly in obese patients, high nursing requirements, severe skin vasoconstriction, or shivering, delayed commencement of the proper temperature, and unpredictable temperature maintenance. Other surface cooling techniques, however, use shallow water circulation and an automatic temperature feedback control mechanism to provide heat exchange. These different methods appear to be more effective than conventional cooling blankets at maintaining the target body temperature with minor variance.

#### 1.2.4.1. Neck Cooling

Some devices are meant to be worn exclusively on the cervix, in the company of the goal of chilling the carotids and, thereby, the brain. Several studies have found that neck cooling techniques are a safe and effective way to cool the brain and achieve moderate hypothermia, which is required for neuroprotection [15, 16].

In some instances, water-circulating Arctic sun pads explicitly made for placing over the carotid triangles were utilized to treat individuals with SAH and intractable fever. Within a few hours, the average temperature of the brain dropped by around 0.5°C, although the drop was not carried over. Emcools have created heat reduction pads to tackle neck cooling; however, they have not yet been thoroughly tested [17].

Gard and his colleagues employed the PolarCap System, which is a high-voltage mobile heat reduction system that uses managed heat reduction of the scalp and neck through a flowing coolant (PolarCap Coolant), to lower brain temperature in ice hockey players [18]. The coolant is continuously changed to maintain a temperature of 0°C in order to prevent outreaching moderate temperatures and to conserve the needed temperature. The PolarCap Coolant is pumped using a head hat made of silicone. To keep the cold out, a neoprene protective gear is placed in addition to the cap. The players were allowed to unwind if they wore the heat reduction head hat and neoprene protective gear. The study procedure recorded the time it took from the injury to the start of treatment and the length of time to calm down. The main finding was that players who received selective neck-head heat reduction immediately following an injury recovered to full game-play much faster compared to those who received a regular cooling procedure.

Cerebral Cooling Collar is similar, with a cold pack that can be removed and worn across the front of the neck. The use of this device in a side-by-side comparison with a systemic surface cooling device for reducing fever in stroke patients in neuro ICUs has been ethically approved. On some healthy volunteers as well as on others who had suffered a stroke or a head injury, this device was examined, and it was discovered that neck-head cooling decreased temperature of the brain without compromising physiological or discernible markers [15].

The above studies imply that non-invasive neck heat reduction devices which hold detachable cold slots above the carotids are outstanding for fast induced brain normothermia and are available on the sideline. These findings, however, should be validated in larger investigations. It's unclear whether these neck cooling gadgets are significantly dissimilar from currently available individual heat reduction neck devices.

1.2.5. Invasive Cooling

Invasive approaches have much fewer human trials than non-invasive treatments. Although it is not fully accurate to report the domain as in its inception, eagerness for it started in the 1960s or 1970s; sadly, that keenness did not last. Invasive approaches are probably an under-researched method of selective hypothermia. Nonetheless, there are a few investigations worth discussing. Invasive cooling techniques are divided into two types: cold oxygenation with respect to the apoplexy and conductive or convective heat conductions from the numerous intracranial partitions. Several invasive heat reduction methods, such as transvascular and compartmental, remove heat from the brain.

Mildly invasive procedures are routinely used in clinical practice to monitor ICP and remove CSF from various cerebral compartments. To convectively cool the brain, Cheng et al. adopted constant epidural irrigation in the company of frozen saline delivered through burr holes [19]. In their pig version, they reached intravenous temperatures of 14°C, subdural temperatures of approximately 20°C, and parenchymal temperatures of 29°C. After starting the cooled saline drip, local hypothermia was achieved in 5 minutes and was easily stabilized for 7 hours. The temperatures of remote brains could not be recorded. In a subhuman ape TBI version employing controlled cortical impact, often termed as CCI, King et al. investigated the effects of a heat reduction device known as the ChillerPad enforced to the dura on brain temperature [20]. The midbrain surface was chilled to around 16°C and kept at that temperature for one day before being rewarmed for about 10 hours. At a depth of 15 mm, brain tem-

peratures dropped to 34 to 35°C at the cortical grey/white juncture and to 27 to 31°C at 9-10 mm. At a distance from the heat removing pad, heat removal quickly dwindled.

In various animal models, compartmental heat reduction techniques have been demonstrated to be successful [19, 20]. These findings can simply be applied to human populations. Epidural cooling techniques, while efficient in cooling the brain locally, might be limited to secluded brain parts due to epidural bonds to the skull. Subdural cooling is an approach that can impact a larger brain section than epidural cooling. The cortical surface is cooled most directly via subarachnoid cooling. Furthermore, subarachnoid cooling can have a global influence on the cerebral vasculature that lies in this area. Intraventricular heat reduction may cause significant drops in the temperature of the brain, but it further has the danger of causing iatrogenic hydrocephalus. Infection and cerebral haemorrhage are additional dangers associated with compartmental cooling techniques.

The field of invasive hypothermia, formerly popular, is in desperate need of a resurgence. Brain cooling may be achieved quickly, reliably, and selectively using invasive procedures. Various invasive approaches to targeted brain cooling have generated encouraging results in animal trials. Human data, on the other hand, is mostly lacking. More human tests and experiments are required. Future research could range from simple, approachable studies like transcutaneous cooling in individuals who have had decompressive craniectomies to increased complicated treatments like intraluminal arterial cooling.

### 1.3. Micro-Heat Exchanger Based Cooling

#### 1.3.1. Micro-Heat Exchanger

The refrigeration and air conditioning system have been studying high reliability and performance heat exchangers. Copper substitution has been a significant worry in recent years due to the increasing call for featherweight materials and spiking copper rates. Aluminium construction is one of the most environmentally responsible options on the market due

to its high strength, sealed design, and recyclable components. By employing aluminium, manufacturing prices can be decreased, and product combativeness might be increased. Micro heat exchangers have been extensively studied and used in electronic equipment cooling. Micro heat exchangers can minimize equipment weight and increase device compactness to meet heat exchange requirements. As process technology improves, micro heat exchangers technology is moderately being utilized in residential air-conditioning and vehicle air-conditioning systems.

Because of structural and other changes, micro heat exchangers have substantially different flow and heat transfer properties than conventional heat exchangers. Scale effects can be blamed for some of the events and new laws that have emerged in Micro-channel. Reduced scale increases fluid compressibility; increased roughness increases drag coefficient; as the surface region to volume proportion increases, the impacts of the driving force related with the zone (viscous or surface forces) in micro-scale channel might be encouraged, and the effect of axial heat conduction of the micro-scale channel wall will be enhanced [21]. The tiny heat exchanger is an ingeniously simple, all-aluminium design that is both lightweight and galvanic corrosion resistant. At least one fluid travels through tubes or enclosed channels, commonly refrigerant or water, while air flows cross-current between the connecting fins.

The pressure drops and heat transmission properties must be precisely forecasted before constructing the micro-heat exchanger. The number and direction of microchannels and the size of the headers alter based on where the heat-exchanger is in the network and which liquids are delivering the heat. Other design improvements aim to reduce condensation, prevent corrosion, and enhance fluid flow. However, it is anticipated that with a more in-depth examination of micro heat exchanger performance, optimization of heat transfer

structure, and the resolution of existing production and application challenges, micro heat exchangers will become more frequently employed.

### 1.3.2. Types of Micro-Heat Exchanger

The various classes of microscale heat-exchangers are identical to those of conventional heat-exchangers. They have one to two paths through which the liquid can travel. When a heat exchanger simply has one fluid and one channel, the fluid is used to transport heat to another site. This heat exchanger is frequently used in automation to transmit heat from the liquid to the automated equipment. When we have two liquids and two channels, the direction in which the fluids flow by each other is commonly used to classify them. Cross flow and counter flow heat exchangers are two types of microscale heat exchangers.

Microscale counter flow heat-exchangers function identically as macroscale counter-flow heat-exchangers do. The two fluids move in opposite directions through a counter flow heat-exchanger. At opposing ends of the heat exchanger, the fluids enter. Because the cooler fluid departs the counter flow nano-scale heat-exchanger at the same point where the heated liquid arrives, the cooler liquid will take aside the hot fluid's entrance temperature. Microscale heat exchangers with a counter flow are further competent than those with a cross-flow.

Cross Flow microscale heat-exchangers are similar to cross flow macroscale heat exchangers in that they work in the same way. One fluid flows perpendicular to the other in a cross flow heat exchanger. One liquid runs along the channels/tubes, while the other liquid flows at a 90° angle around the tubes or channels. Cross flow microscale heat-exchangers are commonly used in two-phase flow practices where one of the liquid changes form. The microscale cross flow heat exchanger is made up of a series of parallel yet short microchannels that work together to achieve significantly larger mass flow rates, minimal pressure drops, and high heat transmission estimates. These microscale heat-exchangers outperform previ-

ously existing macroscale heat exchangers in terms of performance. Channel heights typically range from a few hundred micrometres to roughly 2000 micrometres, and channel widths usually range from 50 micrometres to approximately two hundred micrometres [22]. The implication of microchannels in a cross flow micro heat-exchanger reduces thermal diffusion scales, encouraging far more heat transmission for every one unit mass/volume than has previously been possible. The cross flow microscale heat exchangers outperform macro heat-exchanger structures in terms of performance.

Heat exchangers with working fluids may be used to cool or heat a fluid-fluid or fluid-solid system at varying temperatures, depending on the application. Fluid–fluid heat exchangers can be divided into two classes based on the transfer process. Indirect contact heat exchangers use a solid separating media between the two fluids to heat and cool. The term "surface heat exchangers" is frequently used to describe these. In contrast, direct colliding heat-exchangers are systems that do not physically separate the fluids that flow in the same space.

In heat exchangers that thermally mix fluids, it is critical to be able to enable heat transmission at a less significant energy rate. The larger the merging between the two passages at unlike temperatures, the better effective the thermal merging. As a result, the main goal for this sort of heat exchanger is to identify configurations that improve mixing. Increasing the thermal mixing of fluids travelling through channels, on the other hand, is not cheap. If moving components (such as stirrers and pitching elements) are employed, one must consider the energy required for these devices to function. Active devices comprise parts that consume electrical energy and are difficult to include in microscale applications. However, using static mechanical gadgets, which do not ask for extra energy consumption or the creation of any moving component or structure at the nano-scale, is an option [23]. These are purely passive devices. Grooved channels or putting items in the channel are examples of this type of de-

vice. Despite the fact that these new design components do not require extra feedback energy, the pumping requirement is possibly to be raised as a result of the higher pressure loss caused by the drag force.

### 1.3.3. Efficiency of Micro-Heat Exchanger

Waste heat wastes a lot of energy, notably in the electricity generation and transportation industries. The efficiency of thermal operations can be greatly improved by using heat exchangers. The performance of a micro-channel heat-exchanger used to smother a significant heat flux heater for industrial and microelectronic heat reduction executions was investigated by Nikkhah and his team in an experiment [24]. He came to the conclusion that as the enforced heat flux across the micro-channel grew, so did the heat transmission coefficient. The heat transfer for cooling applications was greatly aided by the thermal conductivity, heat magnitude, and density of water. Overall, the micro heat exchanger demonstrated excellent thermal performance, owing to the higher impact of heat transfer improvement on the system's thermal performance. Microchannel designs allow low thermal conductivity materials to be employed in high-efficiency heat exchangers, resulting in higher efficiencies [25].

### 1.3.4. Benefits of Micro-Heat Exchanger Based Cooling

Micro heat exchangers were first utilized in cooling high-density electronic devices in the 1980s and later in the MEMS (microelectronic mechanics system) industry in the 1990s to meet the rapid development of current microelectronic mechanical heat transfer requirements. With more research into the features of micro-channels and their use in the promotion of electronic cooling, the advantages of micro heat exchangers that a regular heat exchanger cannot match are progressively becoming apparent. Micro heat exchangers eventually made their way into the refrigeration and air conditioning industries. Micro heat exchangers are being used in car air conditioning systems. The technology of micro heat exchangers used in

single-cold air-conditioner condensers has increasingly progressed in the household air conditioner field.

The most significant advantage of adopting micro heat exchangers is their efficiency. In the same space, many compact conduits supply extra surface region for refrigerant-to-wall association than bigger channels. Heat transfer efficiency improves with increased surface area, with some manufacturers claiming improvements of 10 to 35% over the typical fin and tube heat-exchangers [26-28]. Heat transmission in heat-exchangers takes place mainly through conduction across the walls, with convection releasing heat from the centre of the fluid taking longer. The volume of fluid travelling via narrower tubes is reduced. When it comes to transmitting heat, convection plays a minor part. As a result, a more significant proportion of the refrigerant is in touch with the walls to transmit heat, but it also requires less refrigerant to achieve the same level of heat transmission. Micro heat exchangers, according to manufacturers, use 30% less refrigerant. Micro heat exchangers can be up to 35% smaller and scale 60% less than equivalent heat-exchangers since they are so much more efficient. Smaller fans can be employed because of their size and efficiency, lowering the system's overall energy consumption. Smaller fans have the added virtue of being quieter. Micro heat exchangers provide additional layout and design flexibility without worrying about noise objections.

## 1.4. Micro-Heat Exchanger Based Brain Cooling

### 1.4.1. Microchannel Cooling System

Microchannel heat sinks have been found to transmit considerable amounts of heat from tiny volumes but at the cost of somewhat high pumping power. A heat sink made up of a high conductivity substrate with a large number of parallel, small diameter channels are widely used to create micro-channel cooling [29]. These heat sinks are small and light, yet they provide significantly better heat transfer coefficients than their single-phase liquid coun-

terparts by allowing the coolant to undergo a phase change (boiling) throughout the channels. When compared to a single-phase heat sink, the coolant flow rate required to dissipate the same amount of heat is considerably reduced, and the coolant inventory for the entire system is also reduced [30]. By keeping surface temperatures close to the coolant's saturation temperature, two-phase heat sinks also improve temperature uniformity. These characteristics, combined with design simplicity, are key reasons for the popularity of micro-channel heat sinks in high-heat-flux cooling applications.

Microchannel cooling systems make use of microchannels' high heat transfer coefficients and boundary layer effects by evenly spreading coolant parallel to the heated surface. Microchannels achieve an incredibly low resistance at a fraction of the occupied volume; however, droplet impingement cooling can reach a lower value of thermal resistance under an ideal liquid film thickness. Recent research has focused on forced liquid and liquid-vapour convection in microchannel heat sinks [31, 32]. A single microchannel is unlikely to be employed in a realistic cooling system. However, system-level criteria like energy efficiency, weight, volume, manufacturability, material compatibility, and, ultimately, the cost will likely decide their successful integration into commercially viable tiny cooling systems.

The microchannel heat exchanger is made up of many multi channels connected by shared inlet and outlet manifolds. Microchannels are small heat sinks with a standard dimension of 10-200 μm, though they can be as small as 1-3 mm in some situations. Heat transfer rates are improved by increased heat exchange surfaces and micro scale effects. The small scale, on the other hand, increases pressure drops. Depending on the application, pressure drop and surface temperature gradients can be insignificant. At a low cost, patented microchannel matrices may be adapted to any topology or power map. Manifold structures (many layers), jet impingement, and two-phase flows can improve the performance of traditional single-layered microchannels [33]. The goal of a microchannel heat exchanger's design is to

generate the least amount of thermal resistance with the appropriate pressure drop for a given range of heat generation and liquid flowrate. Micro-channels are an essential component of micromachined fluid systems and play a vital role in the creation of small-scale fluid flow devices. Micro-channels and micro-chambers are employed in a variety of sectors, including biochemistry, genetics, physics, and industrial applications, in addition to connecting multiple devices. Understanding the process and fundamental distinctions involved in microscale fluid flow is critical for designing microchannels. The optimal heat exchanger design is obtained by predicting the performance of a given size heat exchanger while varying geometries and the number of microchannels.

### 1.4.2. Types of Microchannels

Channels of varying cross sections and diameters have been employed as heat sinks for a variety of heat transfer applications. Conventional channels, minichannels, microchannels, and nanochannels are the four types of channels [34]. Microchannels, minichannels, and conventional channels are classified using a flow classification technique based on the Knudsen number. By suggesting transition boundaries between nanochannels and microchannels, the general classification method also links to nanoscale phenomena. The classification scheme is designed to serve as a guideline, not to automatically create a set of analytical or empirical methods for a specific situation. Conventional channels have a diameter greater than 3 mm, minichannels have a diameter of 3 mm to 200 μm, microchannels have a diameter of 10 μm to 200 μm, transitional microchannels have a diameter of 10 μm to 1 μm, transitional nanochannels have a diameter of 1 μm to 0.1 μm, and nanochannels have a diameter of less than 0.1 μm. For both single-phase and two-phase applications, the above classification is recommended [35].

The flow of liquid in a microchannel is similar to that of a macrochannel. Because the liquid molecules are tightly coupled, the concept of the mean free route is invalid. The conti-

nuity assumption may no longer be valid for gas flows through microchannels. As the channel diameter shrinks from conventional dimensions to minichannels and microchannels, the relative influence of surface tension, viscous, and inertia forces on the Critical Heat Flux (CHF) mechanism changes. In the absence of any wall surface effects, such as electrokinetic or electroosmotic forces, the flow in minichannels and microchannels is not predicted to undergo any fundamental alterations from the continuum approximation used in macrofluidic applications. Microchannels and Minichannels are found in many biological systems, such as the brain, lung, liver, and kidney, and provide extremely high heat and mass transmission rates [36]. Many high flux cooling applications take advantage of these channels' increased heat transfer capabilities.

### 1.4.3. Performance of Microchannel Cooling System

Heat fluxes generated by an electronics component cause the circuit to surpass its allowed temperature limit. As a result, temperature rise (55 percent) is the leading cause of electronic chip failure, followed by vibration (20 percent), humidity (19 percent), and dust (6 percent) [37]. As a result, engineers face a significant issue in successfully removing heat from electronics chips. Microchannel heat sinks are 50 times more efficient than traditional heat sinks at removing heat. Heat transfer improvement in mini- and microchannels is an appealing option already being used in various applications. Heat transfer is enhanced by secondary fins on the surface (microfins), various channel cross-sections, rough surfaces, and the use of sharp corners for effective liquid drainage in condensing applications.

The course of the fluid passing through a microchannel is represented by its profile. As a result, it primarily has two sorts of profile configurations: straight and wavy. The stream lines created in the straight configuration are explicit, whereas, in the wavy configuration, they are wavy. As a result, adequate fluid mixing happens in wavy rather than straight, which improves heat transfer. Due to the increased area of heat dissipation, the wavy microchannels

improve heat transfer performance. The usage of microchannel in electronic equipment improves the device's performance, life span, and efficacy to a higher level [38]. The thermal resistance is inversely proportional to flow; therefore, as the flow increases, the thermal resistance decreases.

### 1.4.4. Benefits of Micro-Heat Exchanger Based Brain Cooling

Heat transfer coefficients of 30-150 micron flow channels are pretty high. Short flow channels allow coolant to be moved with minimal pressure drop. Heat rejection is aided by high coolant exit temperatures. Higher power input, smaller heat-rejection systems, and tighter packaging are all made possible by high-efficiency heat transmission [39]. Low thermal resistance allows for greater power spike absorption without adding mass to the cold plate. As power is delivered to the coolant more efficiently, coolant inlet temperatures can approach the maximum component temperature. Hot spots and surface temperature gradients can be eliminated by tailoring flow channels to a system's power map. Lower junction temperatures increase the longevity and dependability of crucial system components while maintaining the same flow rate.

Many biological systems have microchannels and minichannels, such as the brain, lung, liver, and kidney, and provide extremely high heat and mass transmission rates [40]. Many high flux cooling applications, such as quick pathogen separation and detection and drug delivery studies, are taking advantage of these channels' increased heat transfer capabilities.

## 1.5. How does cooling the CSF helps with Brain Injury?

The micro heat exchanger is a self-contained device that pumps a cold solution to cool the CSF in the brain. By conduction, the CSF cools the surrounding brain. Cold fluids inserted into the brain's lateral ventricles successfully cool the CSF, lowering brain temperature while maintaining systemic normothermia [41]. During the healing from brain inju-

ries, the CSF is also critical for eliminating high molecular weight waste products and other debris, as well as providing a channel for nutrients and hormones to promote proper brain development.

# Chapter 2. Design of Micro-Heat Exchanger

Under typical design restrictions, the influence of size on heat exchanger performance will be investigated. The design restrictions will be the flow rate, length scale, fluid temperature change, and pressure drop. The rate of CSF generation in humans has traditionally been estimated to be around 0.10-0.40 $\frac{mL}{min}$, or roughly 100-400 $\frac{\mu L}{min}$ [42]. As a result, the micro heat exchanger's flow rate is set to 100-400 $\frac{\mu L}{min}$. Convective heat transfer in a steady state is proportional to the temperature differential between the fluid flow and the wall, as well as the rate of change of this temperature difference. This is a characteristic of exponential decay on a specific length scale. The majority of temperature change and heat transmission occurs within two times the length scale, and total heat transfer is calculated as if the original temperature differential exists over one length.' Longer heating lengths and shorter characteristic lengths characterize water flows.

Artificial Cerebrospinal Fluid (ACSF) and water were used as the heat transfer fluids in the micro heat exchanger. The pressure drop of the water over the heat exchanger can be estimated using the head produced by standard fans. Across a pressure differential of 0.7 inches of water, many fans may produce significant flow rates [43]. To reduce pumping requirements, the water pressure drop should be kept to a minimum. Because this is the temperature that will be used during testing, the input temperature for the water was chosen to be 37°. Since the heat exchanger will be positioned atop a Peltier component for optimal heat transmission, it was designed to be about the size of a credit card. Peltier components typically have a length of 4*4 mm. To circumvent the difficulties of creating a closed-body device, it was later decided to 3D print the heat exchanger. As a result, the 3-D printed PMMA heat exchanger proved a viable option for this study.

2.1. Physical Problem

Consider a fully formed, steady-state laminar flow in a three-dimensional channel with a constant cross-sectional area and perimeter, as shown in Figures 2.1 and 2.2. It is assumed that the flow is incompressible and has constant characteristics. Furthermore, no such gravity, centrifugal, Coriolis, or electromagnetic forces exist. In addition, rarefaction and surface effects are believed to be minor, and the fluid is treated as a continuous fluid. The lid (top plate) is insulated for conservative thermal performance estimations. Individual microchannels and intervening fins are often small in comparison to the overall heat sink dimension, allowing for multiple channels to flow in parallel.

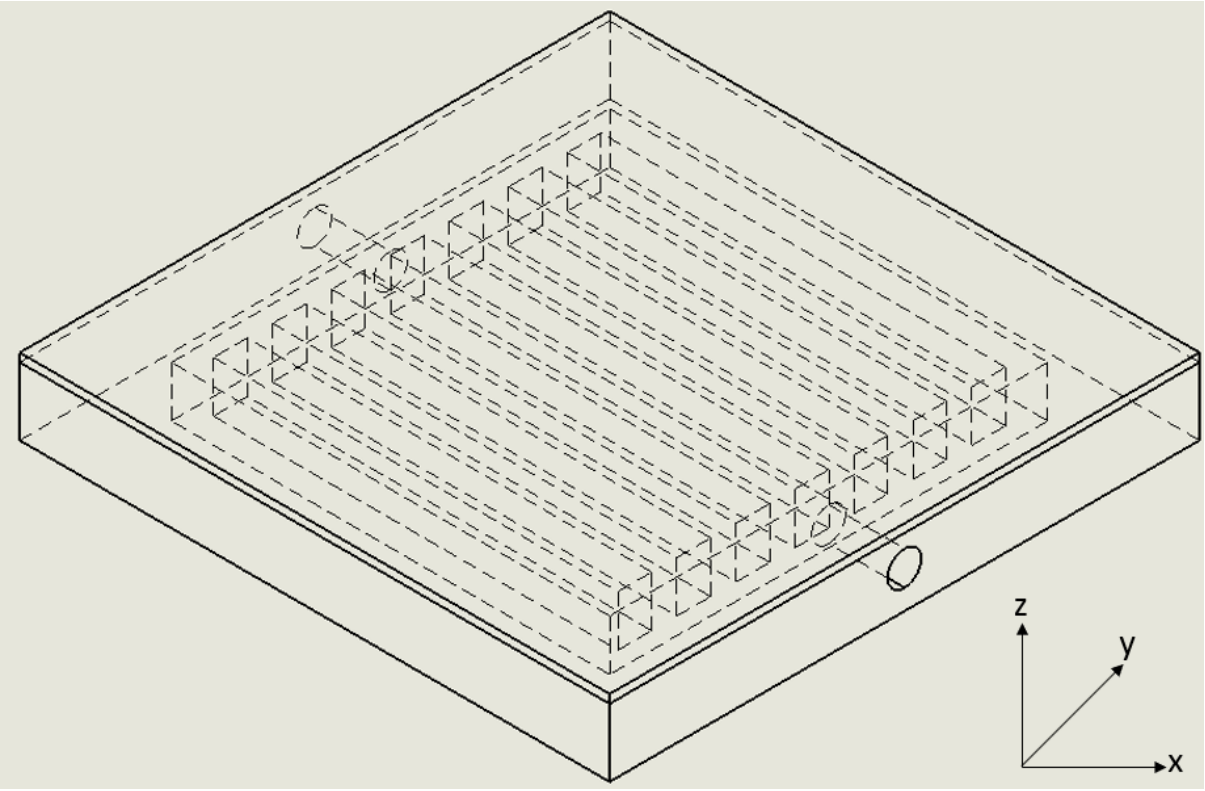


Figure 2.1. Schematic of the microchannel heat sink

The following are the continuum equations [44, 45] for mass, momentum, and energy conservation in convective heat transfer in microchannel heat sinks:

$$\frac{\partial \rho}{\partial t} + \nabla^*(\rho\bar{V}) = 0 \tag{2.1}$$

$$\frac{\partial \rho\bar{V}}{\partial t} + \bar{V}^*\nabla(\rho\bar{V}) = -\nabla P + \nabla^*(\mu\nabla\bar{V}) \tag{2.2}$$

$$(\rho C_p)\left(\frac{\partial a}{\partial t} + \bar{\nabla} * \nabla a_j\right) = \nabla * (K_l \nabla a) \text{ for the liquid} \quad (2.3)$$

$$(\rho C_p)\frac{\partial a}{\partial t} = \nabla * (K_s \nabla a_j) \text{ for the solid} \quad (2.4)$$

Equation 2.1 is based on the continuum hypothesis, which states that a liquid could be thought of as a continuous entity rather than a cluster of separate molecules. Liquids are usually generally considered to be continuous. The interactions between the molecules in the liquid might occur at the same constancy as the interactions between the flow's confinement walls [46]. The renowned Navier-Stokes equation, given after the French physicist Navier along with the Irish physicist Stokes, is found in Equation 2.2 [47]. The Navier-Stokes equations are used to calculate the velocity and pressure field for liquids with continuous viscosity and density. This combination of equations assumes steady-state conditions for incompressible, laminar flow without considering radiation heat transfer. These equations explain the conjugate heat transfer problem in microchannels when used with the right combination of boundary conditions.

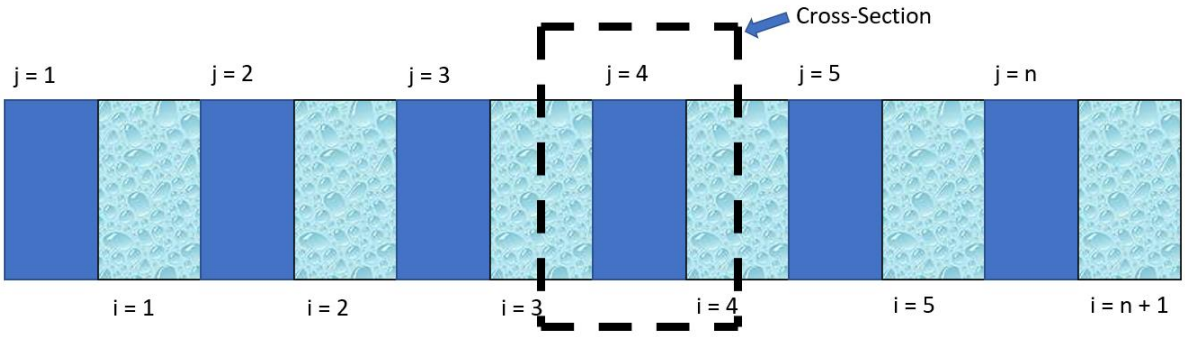


Figure 2.2. Schematic of the cross-section for the analysis

The Reynolds number expresses the relative significance of inertial and viscous processes. The higher the Reynolds number, the greater the dominance of inertial effects over viscous effects. The viscous impacts will dampen out disturbances in the flow path as long as the Reynolds number is not too inflated. Any minor disruption will nourish on the mean flow momentum and develop, triggering new flow formations when the Reynolds number is high enough. According to various modelling studies [48, 49], as the Reynolds number of the hot

and cold sides increases and the input temperature rises, the average heat transfer rate increases. According to the rise in flow rate, this is the typical performance characteristic of the heat exchanger. The pressure drop increases as the Reynolds number of the hot and cold sides increases. The hydraulic diameter and Reynolds number can be computed by using the following formulas:

$$D_h = \frac{4*Area\ of\ the\ Cross-Section}{Perimeter\ of\ the\ Cross-Section} \tag{2.5}$$

$$Re = \frac{\rho*V*D_h}{\mu} \tag{2.6}$$

The average Reynolds number of the flow is often less than 0.01 [50], indicating that CSF motion is creeping flow throughout the majority of the computational area and will therefore obey the model's shape. CSF pressure changes with shape as well, with the cerebral aqueduct having the highest pressure decrease of 1.14 Pa [51]. The flow of CSF is significantly slower in the locations farthest from the inlets; in some cases, the flow is almost static.

2.2. Analytical Model

The convective term is the term $\bar{V}*\nabla(\rho\bar{V})$ in Equation 2.2. The Navier-Stokes equation is nonlinear because of this term. The viscous term, $\nabla*(\mu\nabla\bar{V})$, is also known as the diffusion term. The convective factor can be omitted in diffusion-dominated flows, and the reduced equation is known as the Stokes equation, which is linear. Stokes equations can be used to represent creeping flows or flow with very short length scales (micro or nano flows) with a low Reynolds number. Diffusion-dominated flows are substantially easier to solve numerically than convection-dominated flows, which are often characterized by high Reynolds numbers [52]. A diffusion time scale is better appropriate for diffusion-dominated problems. Scale analysis is an excellent method for estimating the physical quantities studied, or the order of magnitude range, using the basic principles of heat transfer. The solution to the problem of parallel plates for thermally growing flow lays the groundwork for solving different shaped microchannels [53]. Therefore, Equation 2.2 can be non-dimensionalized as:

$$\frac{d\bar{V}^*}{dt^*} = -\nabla P^* + \frac{1}{Re}\nabla^{*2}(\bar{V}^*) \quad (2.7)$$

The dimensionless parameters, Prandtl and Nusselt numbers are used, and the following relations represent them:

$$Nu = \frac{h*D_h}{K} \quad (2.8)$$

$$Pr = \frac{\mu*C_p}{K} \quad (2.9)$$

Because the Prandtl number characterizes the link between the viscosity and thermal conductivity of the fluid, the Reynolds number measures the mixing movement associated with the flow; physical experience indicates that the Nusselt number relies on the Reynolds and Prandtl numbers. The flow's average Prandtl number is frequently less than 4.50, whereas the Nusselt number is around 4.364 [54, 55].

We assumed a laminar, fully developed fluid flow through a heat exchanger made of multiple parallel rectangular channels with an insulated wall. The volume of the heat exchanger scales with the length of the channel since the percentage of total frontal area occupied by the channels is considered to be constant. Regardless of scale, the percentage of total frontal area occupied by the channels is believed to be constant. In other terms, as the size of the channel shrinks, the number of channels per unit area grows. The impacts of the inlet and exit will be ignored. In actuality, there are considerable entrance and exit effects, and fluid flow is frequently not fully developed; therefore, the scaling laws are merely approximate. Energy balances are used in heat exchanger design to determine the rate of heat transfer and all inlet and outlet temperatures required to specify Δa. These energy balances are generally based on flow system equations. The following is the energy balance equation for the liquid:

$$-[(\rho C_p \bar{u}\frac{\partial \bar{a}_i}{\partial z}\Delta z + \rho C_p \overline{ua}_i)W_x W_y - \rho C_p \overline{ua}_i \Delta z W_x W_y + (\frac{\partial q_z}{\partial z}\Delta z + q_z - q_z)W_x W_y + h\Delta z W_y(\bar{a}_i - \bar{a}_j(z)) +$$

$$h\Delta z W_y(\bar{a}_i - \bar{a}_{j+1}(z)) + q'' W_x \Delta z)] = -\rho C_p W_x W_y \Delta z \frac{\partial \bar{a}_i}{\partial t} \quad (2.10)$$

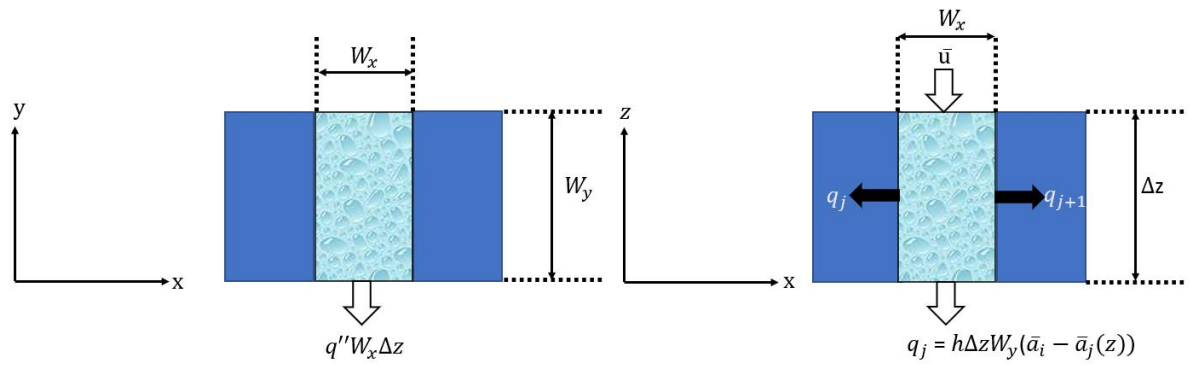


Figure 2.3. Computational domain of microchannel (Liquid)

Equation (2.10) can be reduced further as follows:

$$\rho C_p \frac{\partial \bar{a}_i}{\partial t} + \rho C_p \bar{u} \frac{\partial \bar{a}_i}{\partial z} = K_l \frac{\partial^2 \bar{a}_i}{\partial z^2} - \frac{h}{W_x}(\bar{a}_i - \bar{a}_j(z)) - \frac{h}{W_x}(\bar{a}_i - \bar{a}_{j+1}(z)) - \frac{q''}{W_y} \quad (2.11)$$

where $q_z = -K_l \frac{\partial a}{\partial z}$ is the Fourier law of conduction.

We can assume the temperature-independent liquid properties, and hi is the constant stream-wise function (g(z)). Thus, the following dimensionless variables are used in order to write the energy equation in the dimensionless form:

$$\theta = \frac{\bar{a}_i - a_2}{a_1 - a_2},\ z^* = \frac{z}{W_z},\ t^* = \frac{t}{\frac{W_z}{\bar{u}}} \quad (2.12)$$

$$\frac{\partial \bar{a}_i}{\partial t} = \frac{\bar{u}}{W_z}\frac{\partial \bar{a}_i}{\partial t^*} = \frac{\bar{u}(a_1 - a_2)}{W_z}\frac{\partial \theta}{\partial t^*} \quad (2.13)$$

$$\frac{\partial \bar{a}_i}{\partial z} = \frac{1}{W_z}\frac{\partial \bar{a}_i}{\partial z^*} = \frac{1(a_1 - a_2)}{W_z}\frac{\partial \theta}{\partial z^*} \quad (2.14)$$

$$\frac{\partial^2 \bar{a}_i}{\partial z^2} = \frac{1}{W_z^2}\frac{\partial^2 \bar{a}_i}{\partial z^{*2}} = \frac{1(a_1 - a_2)}{W_z^2}\frac{\partial^2 \theta}{\partial z^{*2}} \quad (2.15)$$

After introducing the dimensionless variables, the governing equation [2.11] becomes:

$$\frac{(a_1 - a_2)\rho C_p \bar{u}}{W_z}\frac{\partial \theta}{\partial t^*} + \frac{\rho C_p \bar{u}(a_1 - a_2)}{W_z}\frac{\partial \theta}{\partial z^*} = \frac{K_l(a_1 - a_2)}{W_z^2}\frac{\partial^2 \theta}{\partial z^{*2}} - \frac{h(a_1 - a_2)}{W_x}\left(\theta + \frac{(a_2 - \bar{a}_j(z))}{(a_2 - a_1)}\right) - \frac{h(a_1 - a_2)}{W_x}\left(\theta + \frac{(a_2 - \bar{a}_{j+1}(z))}{(a_2 - a_1)}\right) - \frac{q''}{W_y} \quad (2.16)$$

After dividing both sides by $\frac{(a_1 - a_2)\rho C_p \bar{u}}{W_z}$, Equation (2.16) can be obtained as below:

$$\frac{\partial \theta}{\partial t^*} + \frac{\partial \theta}{\partial z^*} = \frac{K_l}{\rho C_p \bar{u} W_z}\frac{\partial^2 \theta}{\partial z^{*2}} - h_i \frac{W_z}{W_x}\frac{1}{\rho C_p \bar{u}}(\theta + \varphi_j) - h_i \frac{W_z}{W_x}\frac{1}{\rho C_p \bar{u}}(\theta + \varphi_{j+1}) - q'' \frac{W_z}{W_y}\frac{1}{\rho C_p \bar{u}(a_1 - a_2)} \quad (2.17)$$

where $\varphi_j = \frac{a_2 - \bar{a}_j(z)}{a_2 - a_1}$

Assuming $\frac{K_l}{\rho C_p \bar{u} W_z}$ is small (less than 1), Equation (2.17) can be written as:

$$\frac{\partial \theta}{\partial t^*} + \frac{\partial \theta}{\partial z^*} = -h_i \frac{W_z}{W_x} \frac{1}{\rho C_p \bar{u}}(\theta + \varphi_j) - h_i \frac{W_z}{W_x} \frac{1}{\rho C_p \bar{u}}(\theta + \varphi_{j+1}) - q'' \frac{W_z}{W_y} \frac{1}{\rho C_p \bar{u}(a_1 - a_2)} \quad (2.18)$$

Equation (2.18) is the liquid energy equation. For a steady-state analysis, Equation (2.18) can be transformed, which is as follows:

$$\frac{\partial \theta}{\partial z^*} = -h_i \frac{W_z}{W_x} \frac{1}{\rho C_p \bar{u}}(\theta + \varphi_j) - h_i \frac{W_z}{W_x} \frac{1}{\rho C_p \bar{u}}(\theta + \varphi_{j+1}) - q'' \frac{W_z}{W_y} \frac{1}{\rho C_p \bar{u}(a_1 - a_2)} \quad (2.19)$$

The boundary condition for the fluid is:

$a = a_1$ (First order equation)
Similarly, the following is the energy balance equation for the solid:

$$-[\rho C_p \Delta y W_{xj}(\frac{\partial q_z}{\partial z}\Delta z + q_z - q_z) + \rho C_p \Delta z W_{xj}(\frac{\partial q_y}{\partial y}\Delta y + q_y - q_y) - h\Delta z\Delta y(\bar{a}_i - \bar{a}_j(y,z)) - h\Delta z\Delta y(\bar{a}_{i+1} - \bar{a}_j(y,z))] = \rho C_p \Delta y \Delta z W_{xj} \frac{\partial \bar{a}_j}{\partial t} \quad (2.20)$$

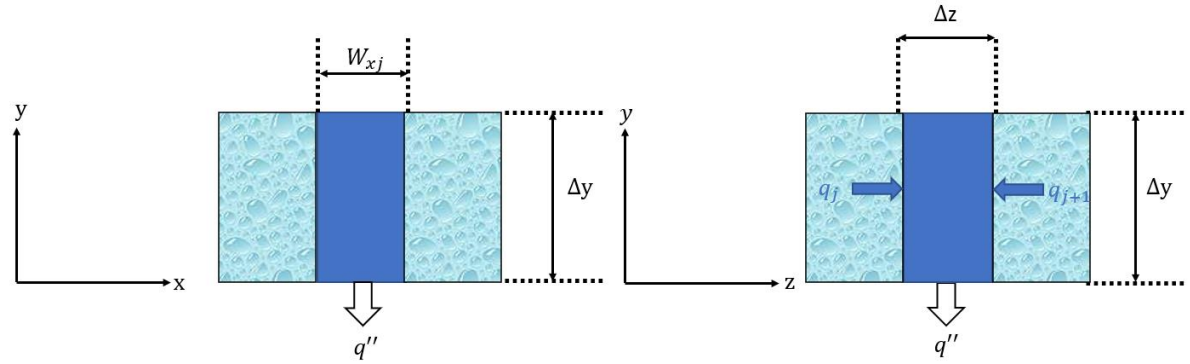


Figure 2.4. Computational domain of microchannel (Solid)

Equation (2.20) can be reduced further as follows:

$$\rho C_p \frac{\partial \bar{a}_j}{\partial t} = K_s \frac{\partial^2 \bar{a}_j}{\partial z^2} + K_s \frac{\partial^2 \bar{a}_j}{\partial y^2} + \frac{h_i}{W_{xj}}(\bar{a}_i - \bar{a}_j(y,z)) + \frac{h_{i+1}}{W_{xj}}(\bar{a}_{i+1} - \bar{a}_j(y,z)) \quad (2.21)$$

We can introduce the following scales and dimensionless variables to Equation (2.21), which will simplify the equation:

$$g(z) \sim W_z \quad (2.22)$$
$$g(y) \sim W_y \quad (2.23)$$
$$z^* = \frac{z}{W_z},\ y^* = \frac{y}{W_y} \quad (2.24)$$

After introducing the dimensionless variables, the governing equation [2.21] becomes:

$$\rho C_p \frac{\partial \bar{a}_j}{\partial t} = \frac{K_s}{W_z^2}\frac{\partial^2 \bar{a}_j}{\partial z^{*2}} + \frac{K_s}{W_y^2}\frac{\partial^2 \bar{a}_j}{\partial y^{*2}} + \frac{h_i}{W_{xj}}(\bar{a}_i - \bar{a}_j(y,z)) + \frac{h_{i+1}}{W_{xj}}(\bar{a}_{i+1} - \bar{a}_j(y,z)) \quad (2.25)$$

Multiplying by $W_y^2$ on both sides, Equation (2.25) can be obtained as below:

$$\rho C_p W_y^2 \frac{\partial \bar{a}_j}{\partial t} = K_s \left(\frac{W_y}{W_z}\right)^2 \frac{\partial^2 \bar{a}_j}{\partial z^{*2}} + K_s \frac{\partial^2 \bar{a}_j}{\partial y^{*2}} + \frac{h_i (W_y^2)}{W_{xj}}(\bar{a}_i - \bar{a}_j(y,z)) + \frac{h_{i+1}}{W_{xj}}\left(\frac{W_y}{W_z}\right)^2(\bar{a}_{i+1} - \bar{a}_j(y,z)) \quad (2.26)$$

Assuming $\left(\frac{W_y}{W_z}\right)^2$ is small compared to other coefficients, Equation (2.26) can be written as follows:

$$\rho C_p \frac{\partial \bar{a}_j}{\partial t} = K_s \frac{\partial^2 \bar{a}_j}{\partial y^{*2}} + \frac{h_i}{W_{xj}}(\bar{a}_i - \bar{a}_j(y,z)) + \frac{h_{i+1}}{W_{xj}}(\bar{a}_{i+1} - \bar{a}_j(y,z)) \quad (2.27)$$

where $\bar{a}_j = f(y,z)$

Equation (2.27) is the solid energy equation. For a steady-state analysis, Equation (2.27) can be transformed, which is as follows:

$$K_s \frac{\partial^2 \bar{a}_j}{\partial y^{*2}} + \frac{h_i}{W_{xj}}(\bar{a}_i - \bar{a}_j(y,z)) + \frac{h_{i+1}}{W_{xj}}(\bar{a}_{i+1} - \bar{a}_j(y,z)) = 0 \quad (2.28)$$

The boundary conditions for the solid are:

1. $-K_s \frac{\partial a}{\partial z} = q''$ (Constant heat flux)
2. $K_s \frac{\partial a}{\partial z} = 0$ (Insulated)

For temperature-independent fluid properties, the heat flux can be obtained using the following balance:

$$\dot{m}_t C_p (a_2 - a_1) = q'' W_z (W_x(n+1) + W_{xj} n) \quad (2.29)$$

Equation (2.29) can be re-arranged to deduce the heat flux as follows:

$$q'' = \frac{\dot{m}_t C_p (a_2 - a_1)}{W_z (W_x(n+1) + W_{xj} n)} \quad (2.30)$$

The impacts of three different control parameters on the flow and heat transfer characteristics, namely fluid flow rate, heat flux, and input temperature, was examined using the analytical solution. The velocity and heat transfer coefficient are affected by the flow rate. The Nusselt number is used to account for the convective heat transfer coefficient. The temperature change of the transfer fluid between the inlet and the outlet decreases as the inlet mass flow rate increases [56]. As a result, the rate of heat removal from the transfer fluid must be raised

to achieve the projected temperature drop of the current experiment. Physically, this will result in a very low temperature for the Peltier component, which is untenable from a practical standpoint. Therefore, the inlet volume flow rate was limited to 100-400 $\frac{\mu L}{min}$ to specify the required rate of heat removal.

## 2.3. CFD Model

Pre-processing, processing, and post-processing are the three general simulation tasks in any computational fluid dynamic (CFD) analysis system [57]. The CFD process used in this study is depicted in Figure 2.5 as a schematic diagram. The pre-processing stage starts with defining and producing the U-type heat exchanger domain's shape and mesh. Following that, the processing step is when the problem's governing equations, numerical models, materials, and boundary conditions are defined. The computations for the solution are then started depending on the given setup. The estimated findings, such as the overall heat transfer rate and thermal profiles, can be automatically viewed and gathered at the post-processing stage. Except for the geometry development, the study's three-step method was carried out using the built-in tools accessible in ANSYS 20.2. ANSYS-Fluent was used to generate the solution for determining the heat transfer enhancement and temperature distribution of the heat exchanger body.

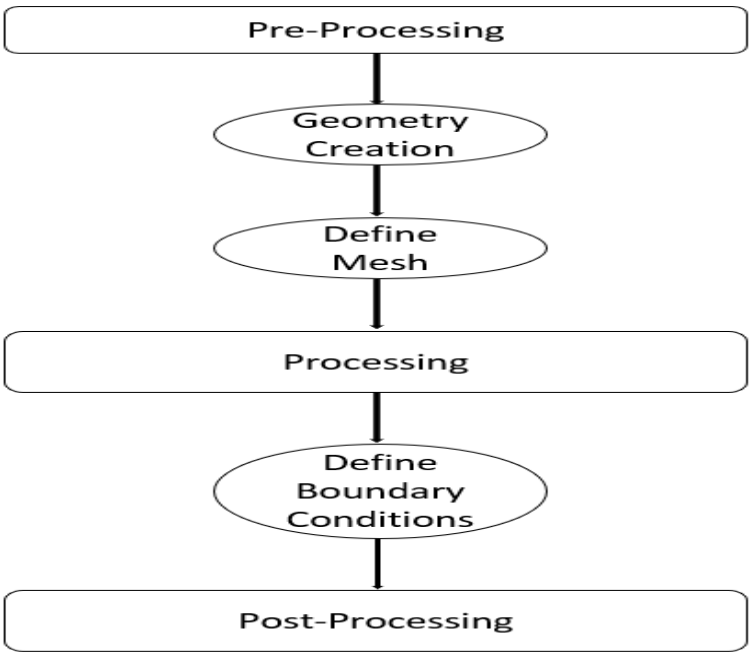


Figure 2.5. CFD analysis steps

The case geometry usually comprises the solid body structure manufactured by design. The fluid domain must be created in order to mimic fluid flow through the heat exchanger. Volume generation methods, such as generation by fluid domain caps or geometric subtraction, can be used to complete the fluid domain generation [58]. Geometric simplifications can also be done during the case geometry creation in more advanced CFD software to reduce the complexity of areas that do not affect the physics of the overall solution. It's critical to establish the geometry of the fluid domains in conjugate heat transfer problems like heat exchanger modelling so that the solid boundaries in contact with the fluid match precisely. The three-dimensional heat exchanger model was created using ANSYS SpaceClaim and then put into the ANSYS Workbench design course for additional processing.

The mesh resolution has a significant impact on the solution in all simulations. Understanding the physics of the problem and performing a mesh convergence study results in a mesh that provides an accurate solution. ANSYS's in-built meshing feature, ICEM CFD, was used for computational meshing. During the numerical simulation, the hexahedral cells that make up the mesh of the overall model will act as data points for the temperature and fluid

flow. The mesh elements and nodes were dispersed across the apparatus utilizing the multi-block structured meshing method. This approach consists of a two-stage procedure. A suitable blocking topology is produced in the first stage, which splits the complicated domain into simple sub-domains. The generated blocks are then meshed together. For topologically simple settings, structured blocking provides an efficient meshing method, and standard templates for partitioning such domains are available [59]. The following are the inputs for the model settings:

Table 2.1. Inputs for the model settings

| **Numerical aspect** | **Solution method** |
|---|---|
| PV coupling | SIMPLEC algorithm |
| Gradient | Green-Gauss Node-Based |
| Pressure | PRESTO! scheme |
| Momentum, Species, Energy (convective) | Second-order upwind |
| Energy | Second-order upwind |

Segregated (sequential solution) and Coupled methods (Simultaneous) are the two most used methods for linking velocity and pressure. The momentum, continuity, and energy equations are solved concurrently and iteratively in the coupled technique. Still, in the segregated method, the modified continuity equation/pressure Poisson equation is employed to solve for pressure using a predictor/corrector approach. Based on the characteristics of both approaches, the segregated strategy is chosen over the coupled approach for the given problem, as the former requires less memory and has a faster convergence time, especially for incompressible and weakly linked problems. The SIMPLEC algorithm is accessible in ANSYS FLUENT. Although SIMPLE is the default, many analyses profit from the usage of SIMPLEC, as this research problem does. SIMPLEC is a method that is similar to SIMPLE. The only difference is the expression employed to rectify the face flow. The SIMPLEC method has been adopted to speed up convergence in issues where the pressure-velocity coupling is the primary barrier to the solution.

Gradients are required not just for computing secondary diffusion terms and velocity derivatives but also for building scalar values at the cell faces. The gradients are calculated using the Green-Gauss Cell-Based, Green-Gauss Node-Based, and Least Squares Cell-Based methods in ANSYS FLUENT. Green-Gauss Node-Based gradients are known to be more accurate than cell-based gradients, especially on complex models, which is why they are employed for this task. Pressure and velocity are kept at cell centres in ANSYS FLUENT's co-located system. As a result, an interpolation strategy is necessary to calculate the face values of pressure using the cell values. There are a few other options for circumstances where the usual pressure interpolation approach isn't viable. However, the PRESTO! (PREssure STaggering Option) system computes the "staggered" (i.e., face) pressure using a discrete continuity equilibrium for a "staggered" control volume around the face. This approach was chosen for this study because it is comparable along to the staggered-grid schemes utilized with structured meshes.

You can choose from numerous upwind schemes in ANSYS FLUENT, including first-order upwind, second-order upwind, power law, and QUICK. Upwinding refers to the face value being generated from quantities in the cell upstream, or "upwind," from the normal velocity direction. When second-order precision is sought, quantities at cell faces are determined utilising a multidimensional linear reconstruction perspective. Higher-order precision is achieved at cell faces utilising this method, which involves a Taylor series extension of the cell-centred solution around the cell centroid. We needed second-order upwind for this research investigation since we wanted higher-order accuracy.

For the steady-state study of the heat exchanger, the time-dependent terms of mass, momentum (x, y, and z planes), and energy are eliminated from the governing equations. It's important to remember that all of the equations shown below are built-in ANSYS CFD solver functions for performing simulations [60].

$$\nabla*(\rho\bar{V}) = 0 \quad (2.31)$$

$$\bar{V}*\nabla(\rho\bar{V}) = -\nabla P + \nabla*(\mu\nabla\bar{V}) \quad (2.32)$$

$$\bar{V}*\nabla(\rho C_p a_j) = \nabla*(K_l\nabla a) \text{ for the liquid} \quad (2.33)$$

$$\nabla*(K_s\nabla a_j) = 0 \text{ for the solid} \quad (2.34)$$

The following table summarizes the boundary constraints applied to the numerical model in ANSYS-FLUENT:

Table 2.2. Boundary conditions

| **Boundary** | **Constraint** |
|---|---|
| Bottom surface | Prescribed temperature |
| All other surfaces | Heat flux is negligible |
| Inlet | Mass flow inlet |
| Outlet | Pressure outlet |

The channel inlet, channel heat exchange walls, and channel outflow are the sites that must be defined. The mass flow inlet condition, which represents the entrance of a single channel, is the first boundary condition that must be met. The channel inlet definition defines the fluid domain faces in the inlet manifold. The heat exchange wall boundaries are the next site to be established. At the bottom wall, the constant surface temperature is specified, while at other external surfaces of the heat exchanger, the heat flux is assumed to be negligible. The pressure outlet condition, which represents the exit of a single channel, is the last of the needed boundary conditions. On the fluid domain faces that represent the channel outlet inside the outlet manifold, outlet pressure is defined. The meshing method requires the provision of all inlet, outlet, and wall locations so that the CFD solver may access them as user-defined boundary conditions.

Based on computational trials, the under-relaxation factor for pressure, velocity and temperature were set at 0.55, 0.4 and 0.7, respectively. From the mesh convergence study, mesh independence was noticed at approximately 2.2 million elements, with mesh biasing/ bunching normal to the wall in the fluid flow path, as shown in the representative mesh Fig-

ure 2.6. Grid sensitivity was used to verify that the solution obtained with the chosen mesh is unaffected by grid size.

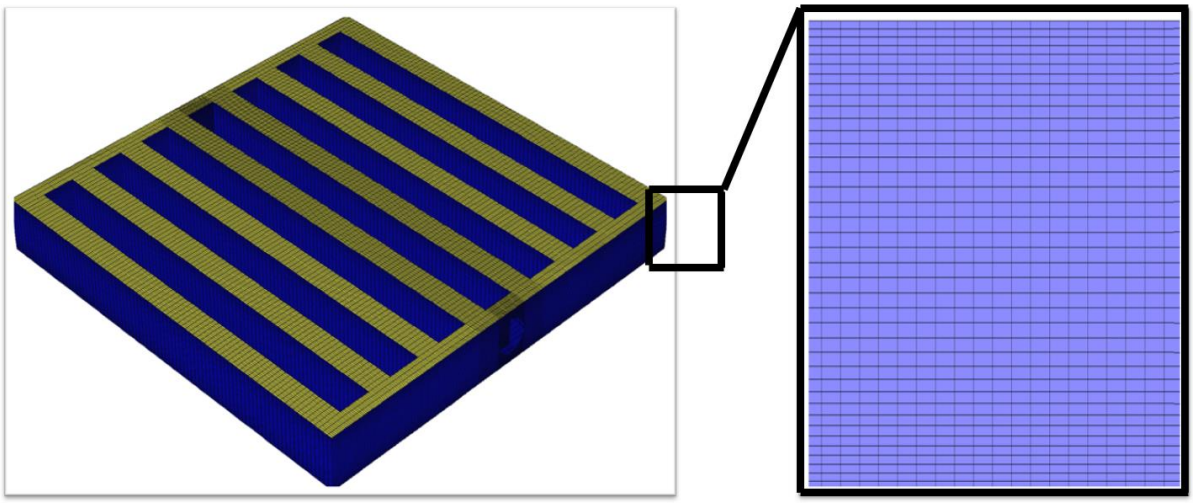

Figure 2.6. Meshed domain along with detail around a corner

The simulation results are processed in the post-processing stage. Based on the simulation results, the overall heat transfer rate, average flow rate across channels and pressure drop between the inlet and outlet are evaluated.

# Chapter 3. Microfabrication of Micro-Heat Exchanger

Manufacturability is one element that determines whether or not a design idea can be realized on a micro-scale. The material preference and fabrication processes utilized for the manufacture of these groups differ greatly because small scale-fabricating methods are often classified to be MEMS (microelectromechanical system) manufacturing or non-MEMS manufacturing [61]. LIGA, Chemical Etching, Stereolithography, and micro-machining are a few of the automations used to blueprint and produce micro-heat exchangers (whether MEMS or non-MEMS) in the company of hydraulic diameters less than 190 micrometres. Micromanufacturing, in general, is the fabrication of objects with functional characteristics or more than one measurement in the micrometre range. As a result, the manufacturing processes used to make the heat exchanger can be categorized as micro-manufacturing.

Because dismantling and construction of small-scale materials are complex, the concept of mending a worn part is unrealistic in small-scale fabrication; instead, substituting the mutilated element with a new one is alternatively economical and practical at this level. Thus, replacing the inlet/outlet in a micro heat exchanger is unnecessary since if the inlet/outlet is broken, the complete heat exchanger is replaced with a new one. As a result, micro and macro heat exchangers cannot be compared in terms of life span. By splitting the complete operation into two mini-operations, "construction" and "production," it is possible to compare design for manufacturing of micro and macro components [62]. While manufacturing possibilities are explored during concept creation, the design process and production can traditionally be divided into two separate activities. However, there is a solid link between construction and manufacture in micro fabrication design, and they should not be examined into two different tasks. This is mostly because microscale dimensions and their impact on production restrictions, limiting the use of most traditional manufacturing procedures such as cutting and shaping.

3.1. Micro-Heat Exchanger Geometry

Figure 3.1 shows the micro-heat exchanger that was created with ANSYS Space-Claim. The dimensions of the micro heat sink are fixed at 35*35*4 mm. The thickness of the base plate was 1 mm. The fins have a rectangular cross-section with a length of 24 mm, a width of 2 mm, and a depth of 3 mm. The channel width is 1.5 mm, while the wall thickness that divides the channels has a width of 2 mm. Eight channels are allowed because enough heat sink edge width is necessary for bonding a cover on top to form the closed fluid flow tunnels. The top cover's dimension is 35*35*0.5mm. Inlet and outlet holes on both ends of the micro-heat exchanger have a radius of 1 mm. The heat sink's fluid flow and heat transmission are predicted to be affected by the inlet/outlet layout.

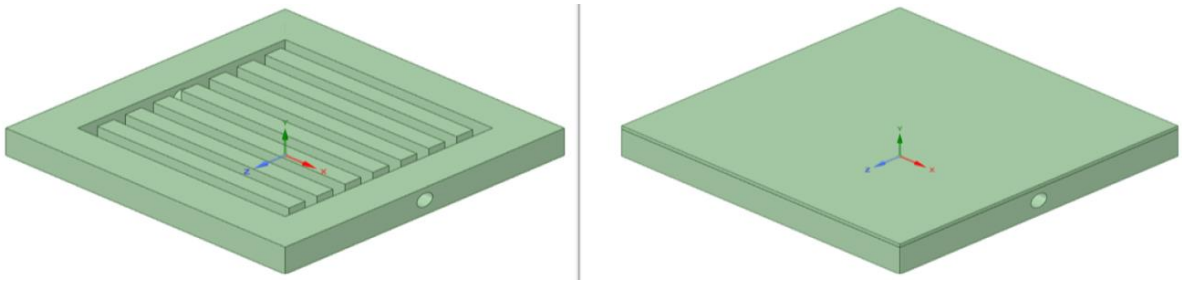

Figure 3.1. Geometry of the microchannel heat sink

Improving heat transfer requires reducing the thickness of the walls. There is less conduction resistance between the fluids and more area for microchannels when the wall width is reduced. The width of the channel is also an essential factor in heat transfer. The number of microchannels and cross-sections can be adjusted by adjusting the channel width and depth. The number of channels can be raised by reducing the channel width. The downside of narrowing the channel width is that it has a lower fluid flow rate, which results in a more significant fluid temperature change (and thus a lower average fluid temperature). In general, using more aggressive design limitations makes fabrication more difficult and reduces the heat exchanger's strength.

3.2. Overview of Fabrication Process

The heat exchanger was manufactured using an EPAX X1 UV LCD Resin 3D printer. This printer may be found in the Fabrication Shop of LSU's Engineering Lab Annex building. The manufacturing process began with the 3D model divided horizontally to plan its layer-based physical assembly. The heat exchanger that must be printed was designed in ANSYS SpaceClaim and then printed as an actual item. The fabrication process is depicted in Figure 3.2.

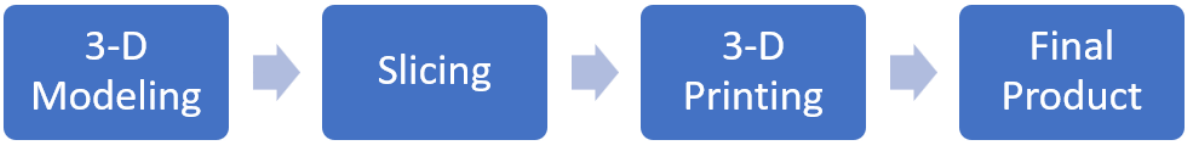


Figure 3.2. Schematic of the fabrication process

To begin 3D printing, we had to first create a blueprint, or three-dimensional digital file, of the heat exchanger. ANSYS SpaceClaim was used to build the design. Finally, before transferring 3D file to the printer, it was made sure that we met a number of design standards. These include characteristics like suitable scale size, minimum wall thickness, manifold/watertight etc.

Next, we had to send the CAD design to the printer once we finished it by converting it into a .STL file. STL stands for STereoLithography and was named after the first-ever 3D printing method. The data that represents the layout/surface of the three-dimensional heat exchanger is stored in this file format as triangular mesh (polygons). The file format had to meet specific requirements, such as a maximum polygon count, watertightness, physical size, and minimum wall thickness.

Afterwards, we had to use Slicing software, ChituBox, to slice our model. Slicing is converting a 3D file into instructions that a 3D printer can follow. Slicing is the process of dividing or chopping a 3D model into hundreds or thousands of horizontal levels and instructing the machine step by step on what to do. After the file was Sliced, a new file format called

G-code with the extension .gcode was created. G-code is a numerical code programming language that is mainly used in computer-aided manufacturing to manage automated machine tools such as 3D printers and CNCs (Computer Numerical Controls).

Then the 3D printing process was initiated. The 3D printing machine needed to be correctly maintained and calibrated to create good prints. After the printing had started, the machine followed the automated G-code instructions. Once the printing was completed, we removed the finished component from the printer.

Finally, to improve the strength of the 3D printed heat exchanger, it was immersed in an epoxy setup for around 15 minutes for post-processing. After that, the heat exchanger was left undisturbed for the next 24 hours to allow it to improve its mechanical properties.

### 3.3. Procedure

When a laser arrives at the tar, the EPAX X1 UV LCD Resin 3D printer uses a liquid-based process to reduce or solidify a photosensitive polymer. This 3D printer's main classification is that it creates object layers by hardening a fluid sap called Ultraviolet (UV) resin that solidifies when exposed to the UV light source. Inside a tank of UV resin, the 3D printer creates object layers. Stereolithography (SLA) and direct light processing (DLP) are the two basic liquid-based systems categories [63]. The SLA technology is used in the EPAX X1 UV LCD Resin 3D printer.

The SLA approach is graphically illustrated in Figure 3.3. SLA is a laser-based method that uses UV resins that react with the light beam and cure to form a solid in a highly precise manner, producing extremely precise parts [64]. The UV resin is held in a vat. According to the 3D data supplied to the machine by the .STL file, a light beam is directed in the X-Y axes across the surface of the resin, where the resin hardens precisely where the light beam touches the surface. The elevator presses down the created layer and then rises to form the

next layer once the previous one is completed. This process of creating layers is repeated until the entire object has been completed.

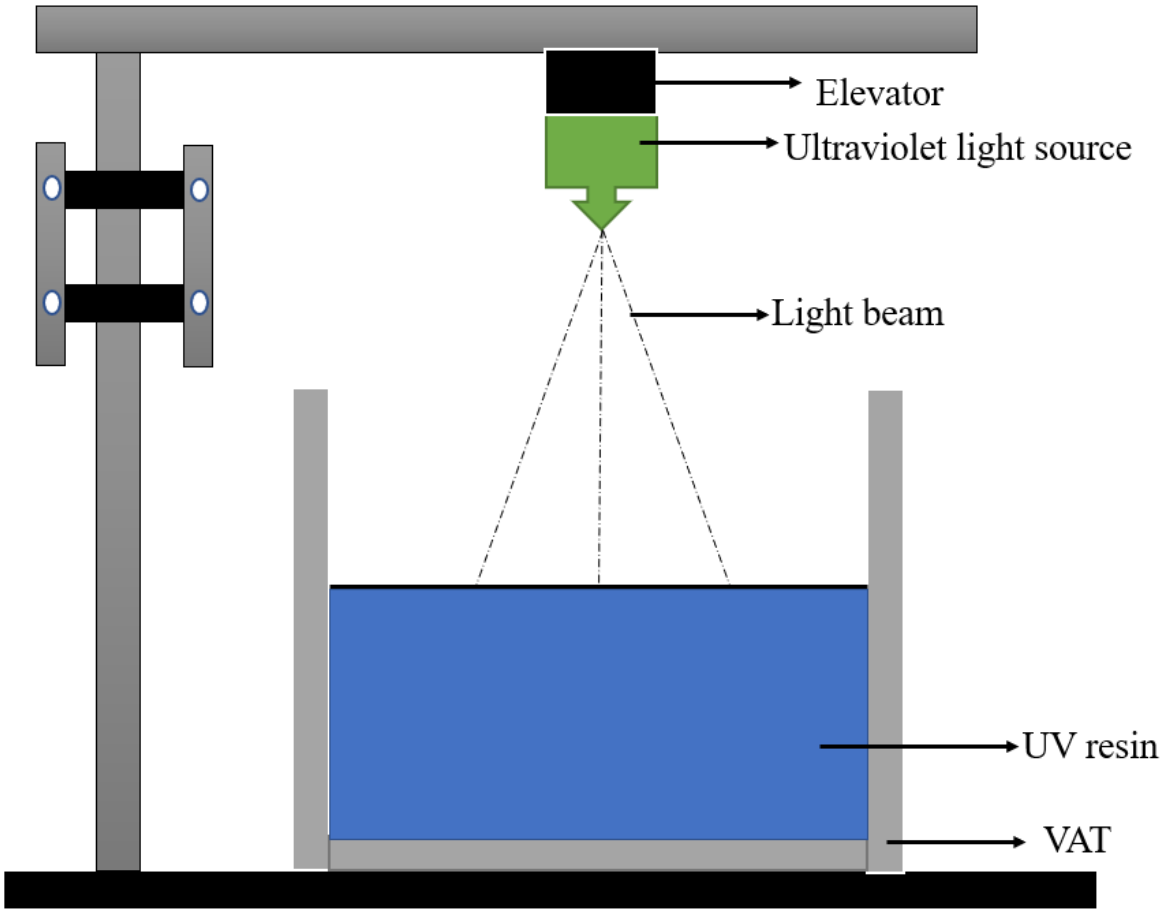


Figure 3.3. Schematic of the SLA method

The SLA method necessitated the use of support structures in order to create a perfectly formed heat exchanger. After the printing was completed, these constructions had to be manually removed. The heat exchanger needs to be cleaned and cured, among other post-processing operations. The heat exchanger was exposed to intense light in an oven-like machine to cure the resin thoroughly. Stereolithography is widely regarded as one of the most precise 3D printing technologies available, with high surface polish [65]. Stereolithography provides several advantages, including the capacity to build complex parts quickly, high accuracy, high thermal endurance, and the ability to use 3D printed objects as templates for casting [66].

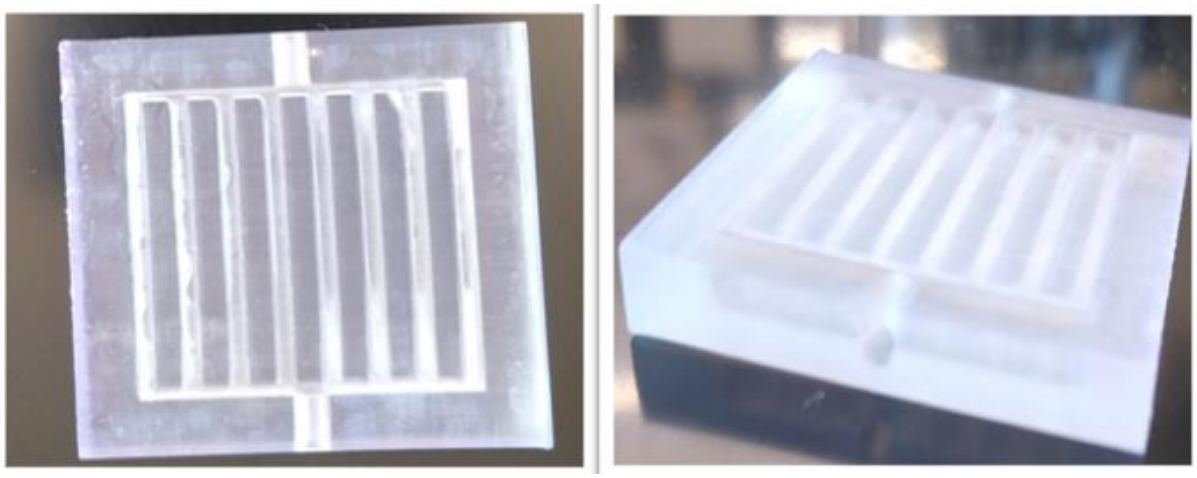

Figure 3.4. Microchannel Heat Exchanger

UV resin was chosen as the material for the heat exchanger because it is perfect for producing high-accuracy prints. UV resin is a robust and long-lasting resin with engineering material properties that make it simple to print on LCD 3D printers. UV resin printing allows practical models to have high impact and accurate prints right out of the printer. We used Anycubic's 3d printing UV sensitive resin as it prints sturdy items with slight shrinkage and a smooth, lustrous surface finish. Figure 3.4 shows the micro-heat exchanger that was obtained using the printing process.

# Chapter 4. System Integration of Micro-Heat Exchanger

In this chapter, the overall setup of the micro-heat exchanger is discussed, which was used to carry out the experiments. Initially, an aluminium-based micro-heat exchanger was explicitly created; however, the material caused significant heat losses. Figure 4.1 shows the heat exchanger that was initially utilized. Fluid flow and heat transmission were investigated in the aluminium-based micro-heat exchanger with rectangular fins. As a result, in order to overcome the heat losses, a polymer-based model was later planned and built. The temperatures at the surface and outlet of the micro-heat exchanger were measured using thermocouples. Because the dimensions are so small, it was required to design a custom temperature measurement system using commercial thermocouples.

Figure 4.1. Aluminium-Based Microchannel Heat Exchanger

The initial experiments to determine the heat exchanger's efficiency were conducted with water as the test fluid. In the micro-heat exchanger, preliminary testing involved confirming the effect of varying flow rates and inlet temperatures. Internal and external leaks were also checked on the micro-heat exchanger to ensure it didn't have any minor cracks that couldn't be seen physically. Finally, we compared the experimental and simulated outcomes to evaluate how well they corresponded.

4.1. Pump Selection

The pumping needs, as well as the pump's compatibility for the microchannel heat sink design, were studied in order to select the best pump. Figure 4.2 depicts the chosen syringe pump, the NE-500 Programmable OEM Syringe Pump. The flow rate and temperature change are the most important considerations when selecting the right pump. There will be a balance in terms of heat gain and loss.

Figure 4.2. Syringe Pumping System

The most critical factor is the temperature difference between the two streams of water on either side of the heat exchanger. The heat exchange surface area must increase as the driving force decreases to achieve heat transfer. Micropumps can be utilized for the heat sink

with 100 μm wide microchannels; however, to obtain the significant pressure drops in these tiny channels, multiple micropumps must be connected in series [67, 68]. For example, if each additional micropump increases the overall pressure head by the same amount without reducing the flow rate, 50 such sets would need to be connected in series for the rotating micropumps combined parallel set. To accomplish the requisite flow rate and pressure head, a total of 50,000 (50×1000) rotary micropumps would be required. Such combination pumps would then have a volume greater than the smallest conventional pump examined. It's also unclear whether such a vast number of micropumps can be implemented in a series-parallel configuration. As a result, when constructing the heat exchanger to match the pump's specific heat removal rate requirements, the ideal size of the microchannels was chosen. At 200 μm microchannel width, the pumping needs of the microchannel heat sink are minimal for the given heat removal rate and thermal restrictions.

4.2. Micro-Heat Exchanger Connectivity with Components

The efficacy of the design was checked by comparing the temperatures of the entering and departing water. The heat exchanger configuration is shown in Figure 4.3. To improve accuracy, the temperature difference between identical temperature flows was monitored rather than the absolute temperatures. A more significant initial temperature differential will result in a lesser per cent error for a given absolute precision [69]. The voltage alarm, controller, cold joint correction, thermocouple, data collector, and gauge contribute to the temperature measurement error. The gross error for final temperature evaluation was calculated to be 0.1°C, considering that all inaccuracies are unrelated. For each data point, the per cent error was determined. The temperature of the syringe might also change over time. Temperature differences over the flow’s cross section at the hot and cold exits, on the other hand, should not produce considerable inaccuracy [70].

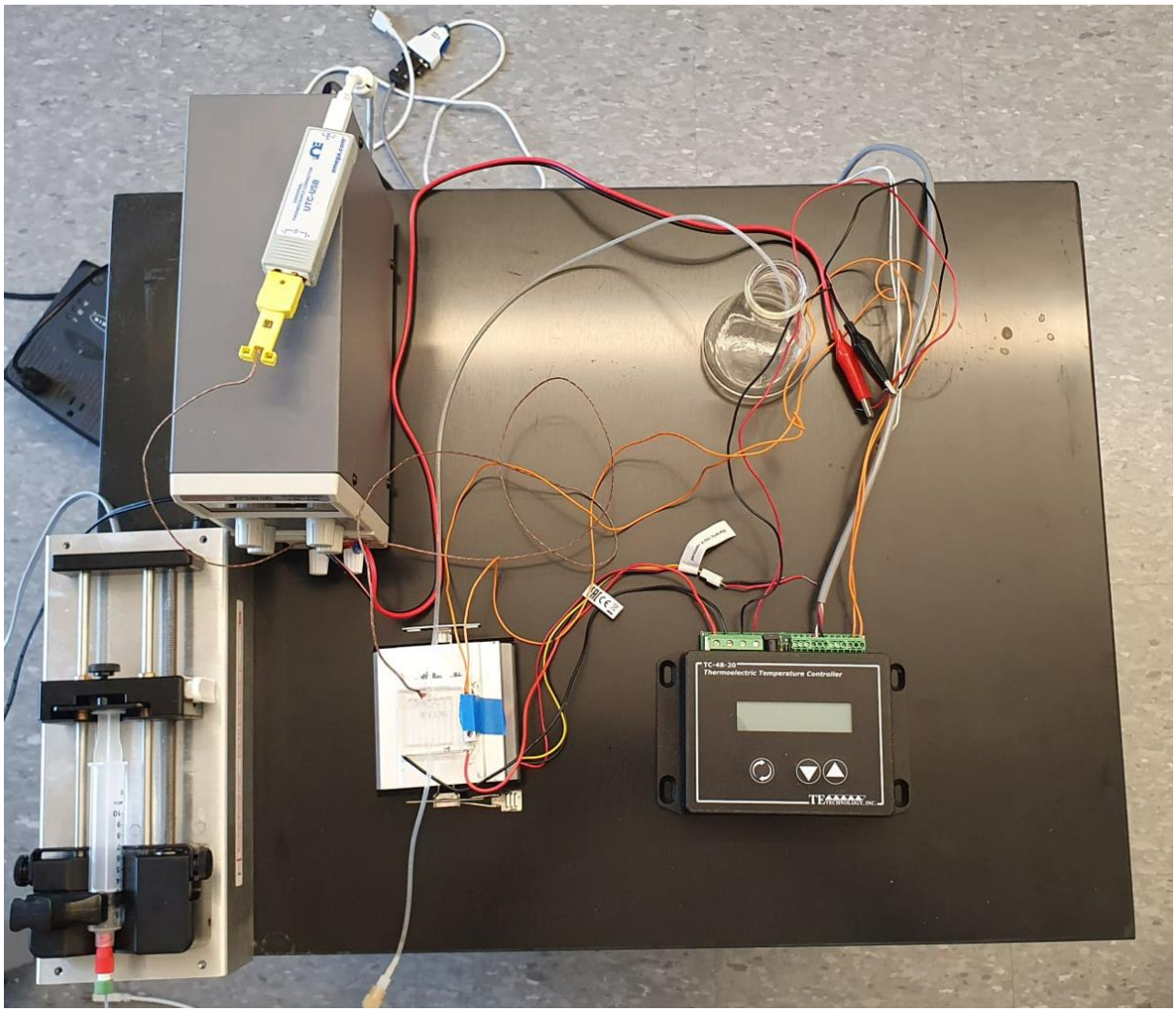


Figure 4.3. Heat Exchanger System Setup

For most flow rates, the total inaccuracy in the flow rate was less than 1%. Bubbles in the heat exchanger are another experimental concern. The inlet's hot water would not form bubbles above cooling because the solubility of gases in water reduces with increasing temperature. Another concern is the likelihood that the heat exchanger had bubbles before the experiment began. To get rid of them, deaerated cold water was poured into the heat exchanger and allowed to run for around 9 hours, which should have been enough time to absorb the bubbles in the mean flow channels. To reduce polymer distortion error, the testing pressure settings were controlled for a few days prior to data collection. With the syringe pump, precise flow control was achievable. As a result, in all runs, the flow was adequately balanced.

4.2.1. Connection with Thermocouple

The experimentally determined heat transfer coefficient depends on accurate temperature measurements at the fluid's inlet and outflow and the surface. As we have seen, the Nusselt number is highly reliant on precise temperature measurements. For a microchannel heat exchanger, this can be pretty difficult. Measuring the surface and exit fluid temperatures is one way. Traditional thermocouples are enormous by contrast and must be placed a set distance from the actual outlet of the microchannel, which reduces their accuracy [71]. This problem can be solved by integrating a micro-thermocouple into the outlet's top surface. Figure 4.4 shows two extremely small thermocouples, one embedded in the heat exchanger outlet and the other sitting next to the heat exchanger. The outlet's thermocouple was strongly glued to keep it stable and prevent leakage.

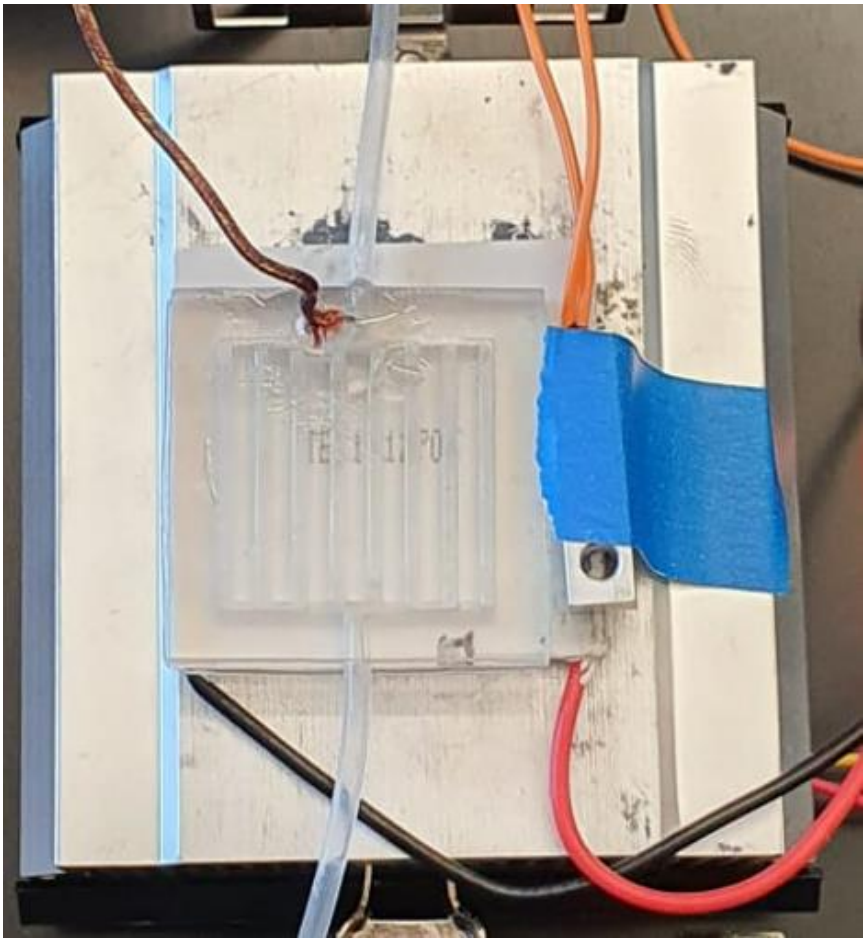

Figure 4.4. Thermocouples

The sensing bead of a thermocouple can be about the same size as the microchannel [72]. Using a thermocouple at the outlet instead of a single channel temperature measurement device is preferable for determining the average temperature at the outlet. Additionally, extreme attention must be used to ensure that the bead does not restrict the flow distribution in the manifold and that the flow is properly mixed at the measuring point.

4.2.2. Connection with Thermoelectric Cooler (TEC)

When a current flows through the junction, heat must be continuously provided to or rejected from the body to maintain the junction temperatures constant. The quantity of current supplied determines the overall amount of heat added or rejected [73]. The Peltier effect is the name for this phenomenon.

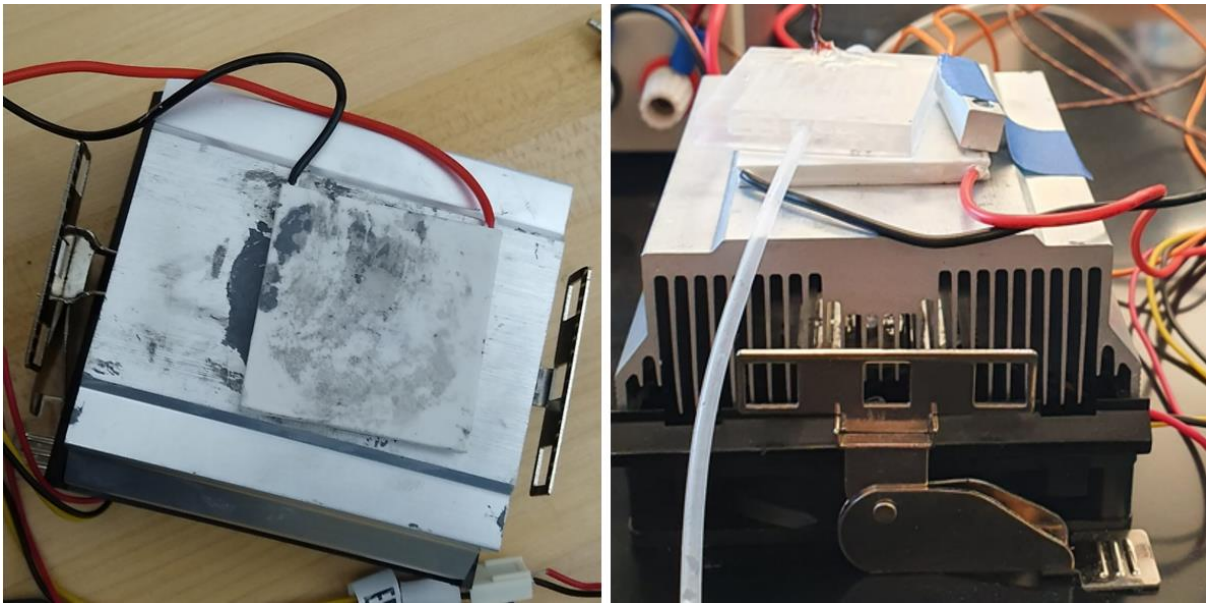

Figure 4.5. TEC/Peltier Component

A thermoelectric pair is made up of a p-type and n-type semiconductor and copper to connect them. When the electric current is applied to an n-type semiconductor in a thermoelectric cooler, heat is absorbed and delivered to the hot side. As a result, there is a general cooling effect. When current is applied in the other direction, the module has the opposite impact and heats up. This concept has a number of advantages over commercial refrigerators and heat pumps, including direct energy conversion, high dependability, cheap maintenance,

and the absence of refrigerants, all of which are true since the thermoelectric cooler is a solid-state device. The thermoelectric module is linked to the heat exchanger and placed on the heat sink, and the configuration can be seen in Figure 4.5. A Peltier component/element is another name for a thermoelectric module.

4.2.3. Connection with Pump

The fluid is delivered to the microchannels through a syringe pump at constant flow rates with no pressure variations. The pump's flow rate is set on the computer that controls the pumping system, and the syringe pushes the fluid forward. Figure 4.6 depicts a schematic layout of the syringe pump configuration employed in this study, which comprises two primary components: the tubing and the pump.

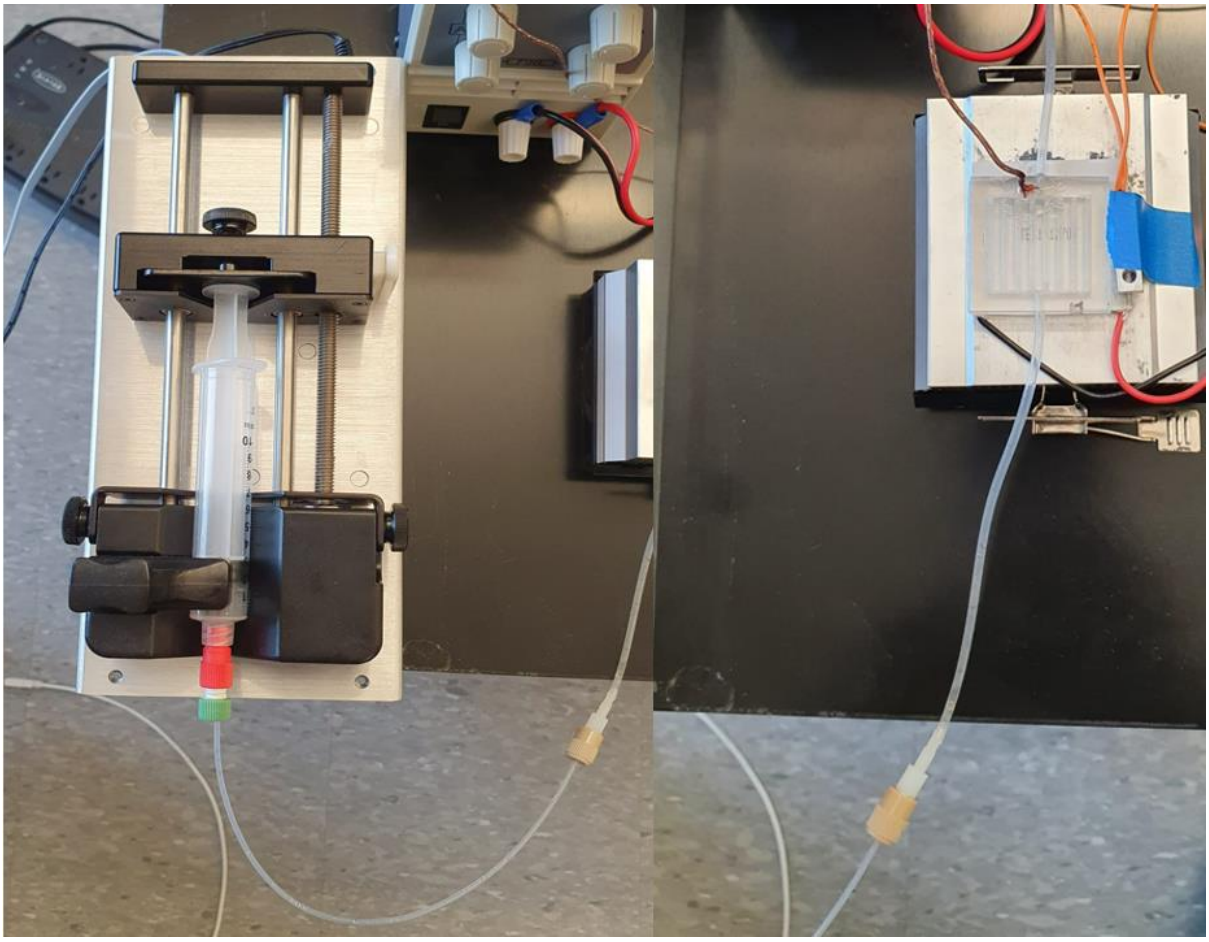

Figure 4.6. Syringe Pump with Tubing

4.2.4. Connection with Temperature Controller

The given fluid temperature management system is based on a TC-48-20 temperature controller, which can be seen in Figure 4.7. The TC-48-20 controller uses pulse-width modulation (PWM) to manage the output power to the thermoelectric cooler. It can handle voltages of 0 to 50 volts and currents of up to 20 amps. The MP-3193 thermistor included with the TC-48-20 provided a temperature control range of -20 C to +100 C. Using the supplied software, the controller was also connected to a computer via an RS232 serial interface for data graphing and logging.

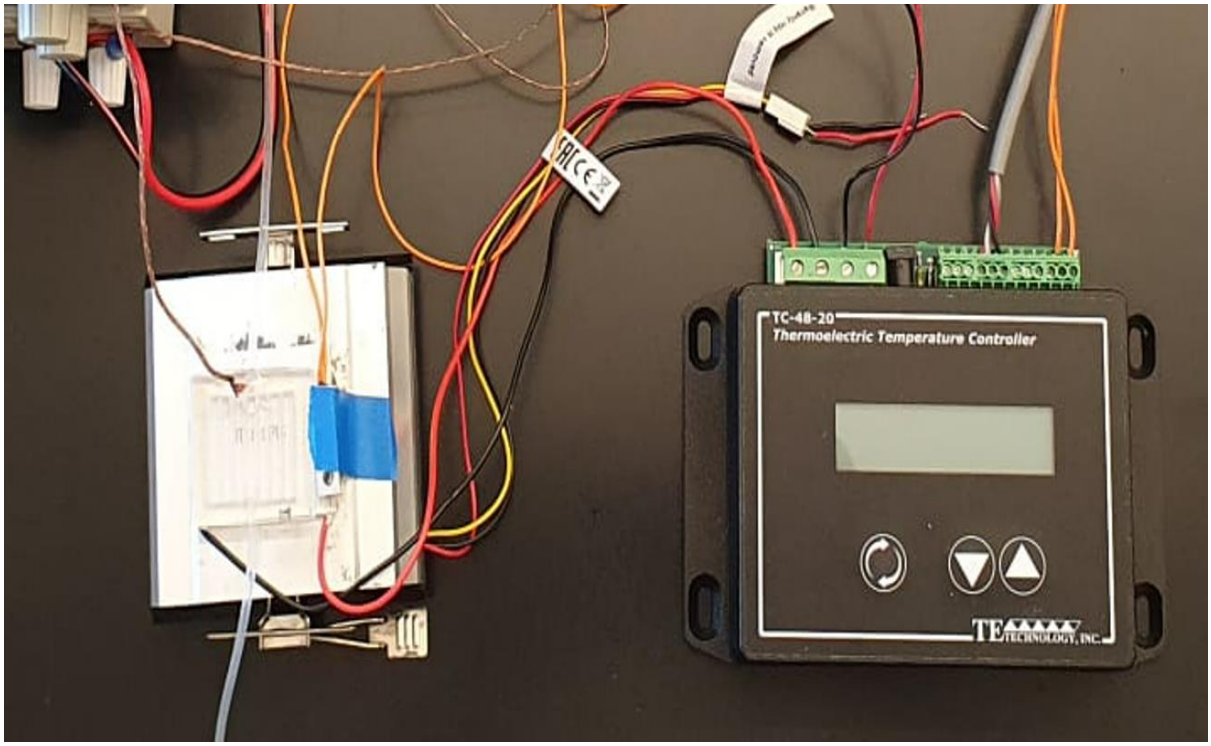


Figure 4.7. Temperature Controller

An Eventek KPS3010D supplied a stable regulated DC power supply that allowed for continuous adjustment of the output voltage and output current levels. The power source in use is depicted in Figure 4.8. Improvements to the heat exchanger design, such as heat exchange efficiency (to raise the heat transfer coefficient) and heat transfer mode (thermal conductivity and convection heat transfer), are made possible with the temperature control system.

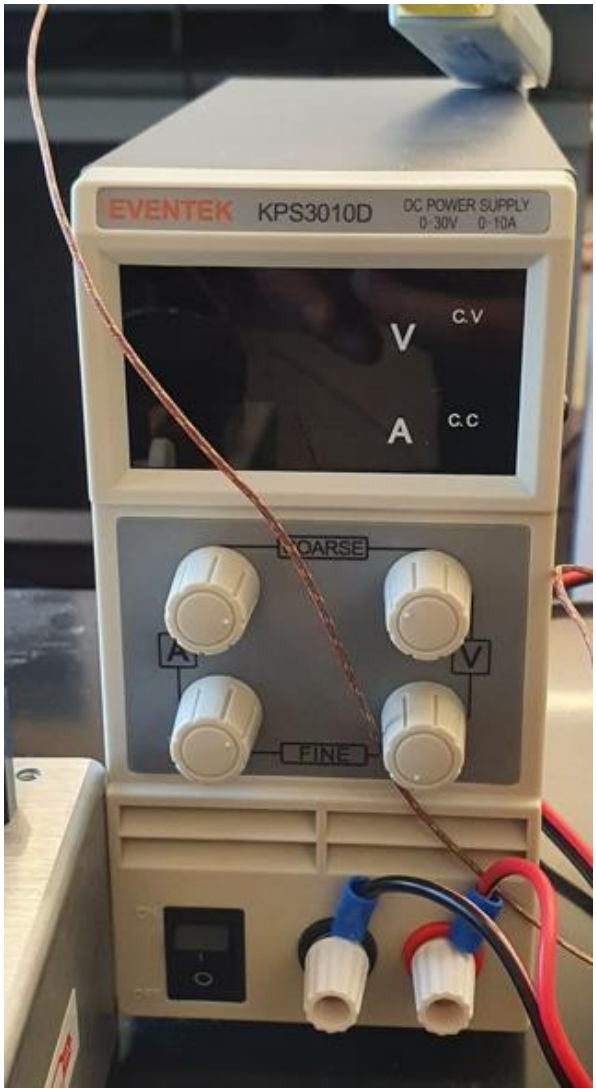


Figure 4.8. DC Power Supply

4.3. Results

After reading some material and comparing several designs, the U-type heat exchanger was chosen. Since the U and V type designs produced noticeably better outcomes than any other design, they were specifically examined in more detail. The shape, average fluid temperature, and average fluid velocity over the channels are shown in Figures 4.9, 4.10, and 4.11. The fluid temperature and velocity are more even/symmetric for the U-type design.

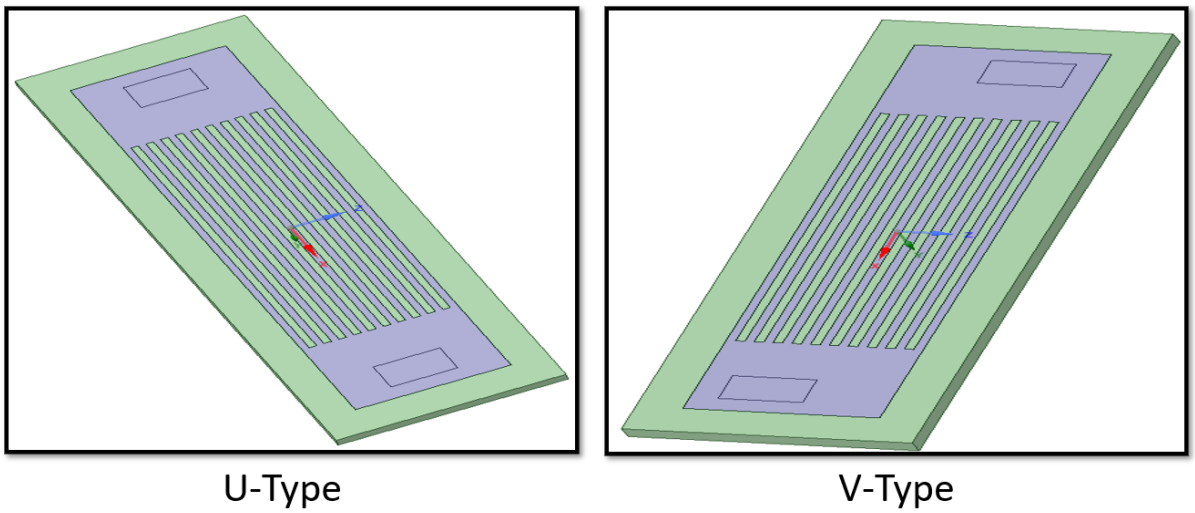


Figure 4.9. U and V type designs geometry

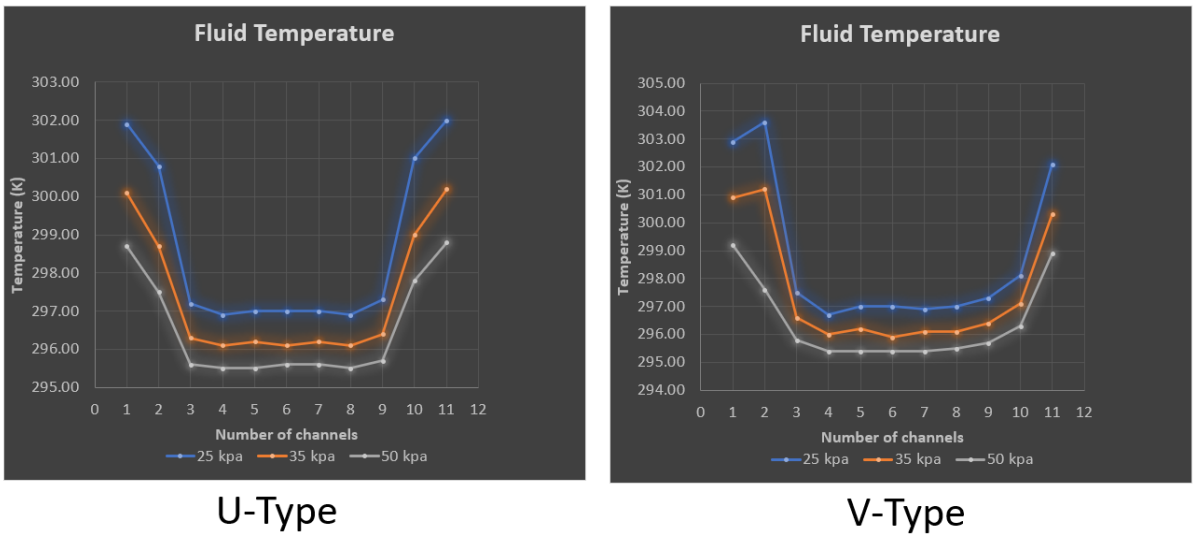


Figure 4.10. U and V type designs fluid temperature

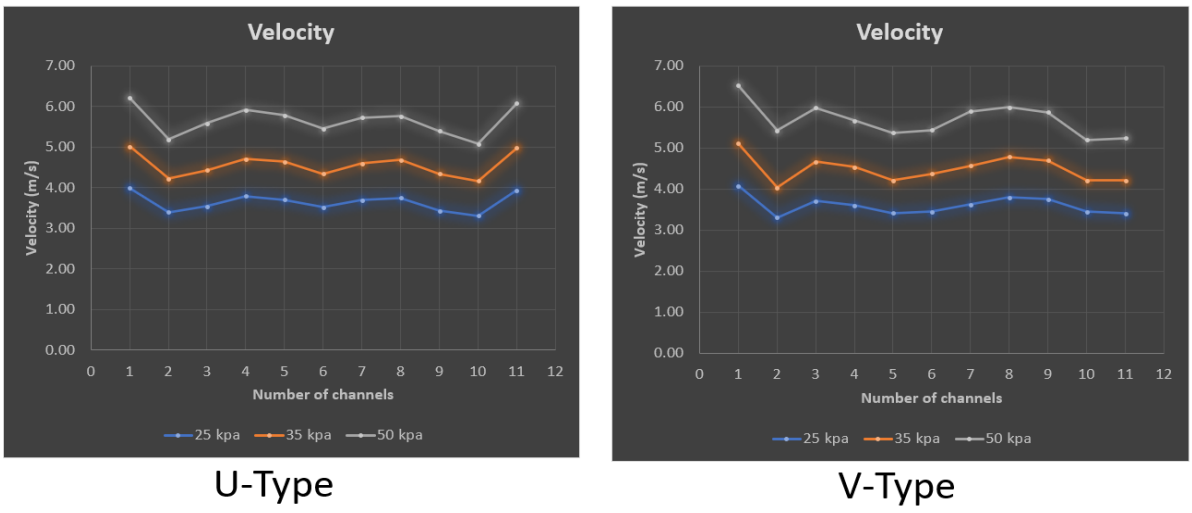


Figure 4.11. U and V type designs fluid velocity

It was also intriguing to find out if the base plate thickness had any bearing on the liquid cooling. In order to determine how long it takes for the fluid to cool from 37°C to 36-33°C, we varied the base thickness between 0.1-1mm with an increment of 0.1 mm. The results shown in Figure 4.12 led us to the conclusion that the base thickness has little to no impact on liquid cooling.

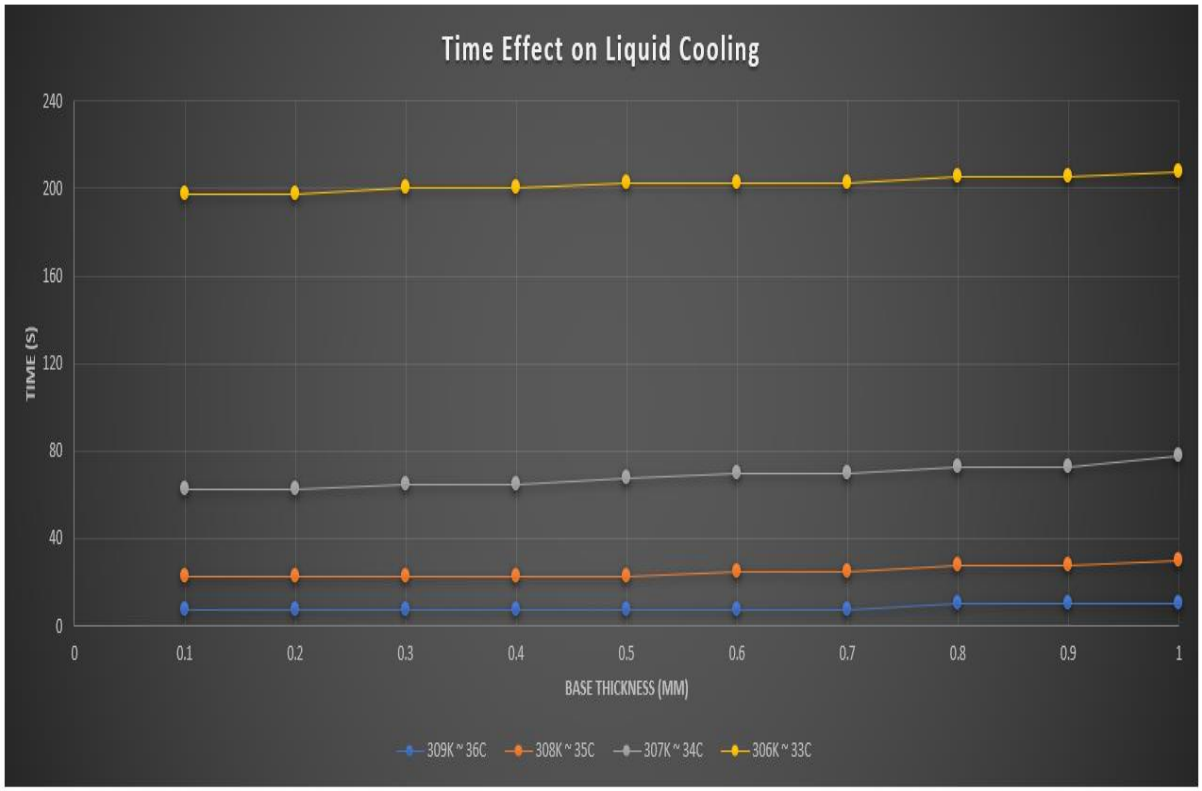


Figure 4.12. Base thickness effect results

It is crucial to check how efficiently the Peltier component manages its temperature before performing any experiment. The findings of the Peltier are shown in Figures 4.13 and 4.14. For one case, we varied the temperature from room temperature to 40°C, 35°C, and 30°C; for the other, we increased the temperature from room temperature to 40°C, then went from 40°C to 38°C and 38°C to 36°C. Both cases produced stable results. Thus, we conclude that the surface temperature maintains its intended temperature over time.

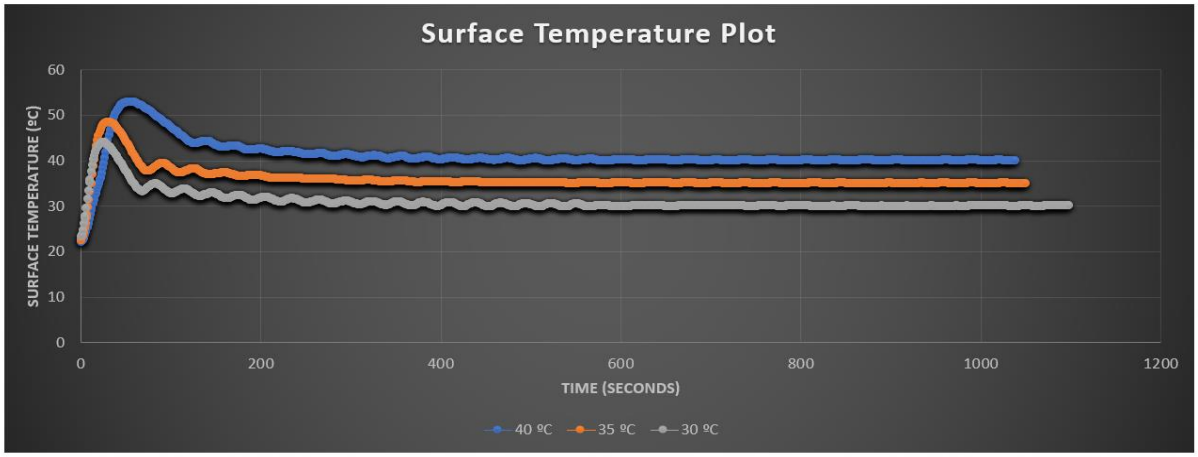


Figure 4.13. Peltier case one

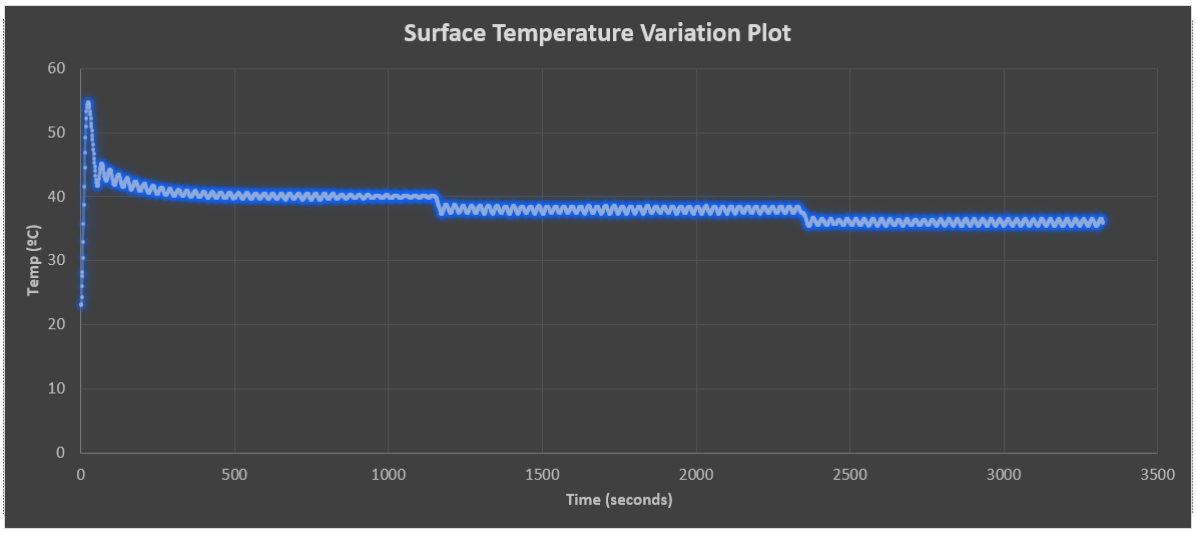


Figure 4.14. Peltier case two

In order to better comprehend the relationship between the surface and outflow temperatures, we decided to examine it. The surface and outlet temperature drop over time, as seen in Figure 4.15. As a result, there is a positive correlation between the two variables.

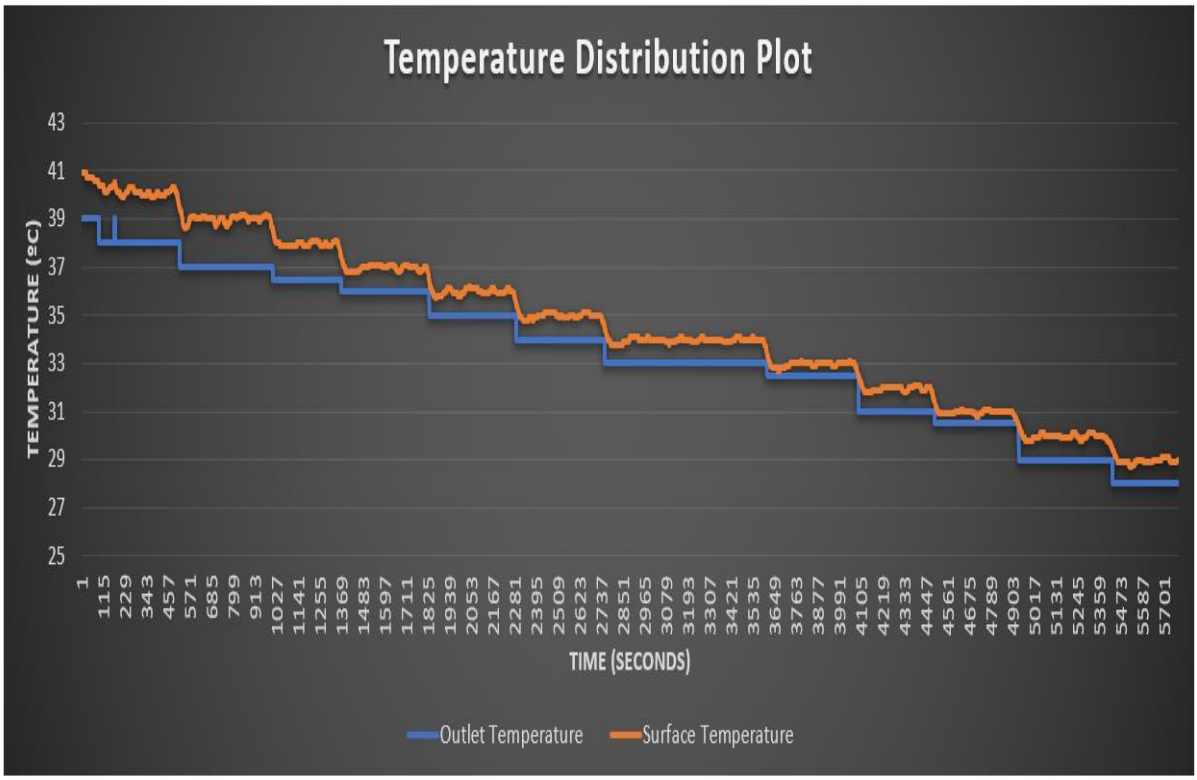


Figure 4.15. Temperature behaviour

The experimental setup was utilised to evaluate the effects of varying flow rates and different outlet temperatures for this work. 100, 200, and 300 $\frac{\mu L}{min}$ flow rates were used, with outlet temperatures ranging from 28 to 35 °C. In all cases, the inlet temperature was 37°C. 2 mL of artificial cerebrospinal fluid (ACSF) was allowed to pass via the heat exchanger. The thermodynamics of the system, which includes a 7.5 W heat source to simulate body activity and a heat exchanger regulated by the Peltier component/TEC, control the temperature of the ACSF. A computer system was in charge of the flow rate. The temperature regulator controlled the temperature of the TEC. The micro heat exchanger's surface and outlet temperatures were measured. Figure 4.16 depicts the principal effect of flow rate on fluid temperature under the experimental conditions.

Flow rate = 100 $\frac{\mu L}{min}$ Flow rate = 200 $\frac{\mu L}{min}$ Flow rate = 300 $\frac{\mu L}{min}$

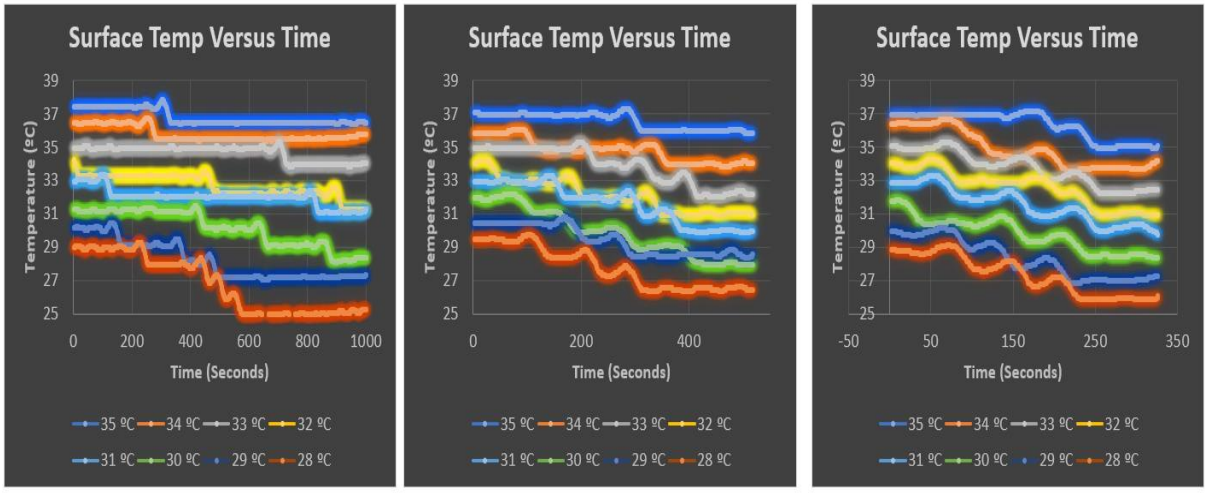


Figure 4.16. Experimental results

Figure 4.17 shows the primary effect that flow rate has on the temperature of the fluid in a simulation with varying flow rates under the same experimental settings. Lower flow rates imply lower velocities inside the heat exchanger and hence the longer time spent in a heat-transfer-friendly environment. Individual fluid particles spend less time within the heat exchanger as the flow rate increases, and there is less time for the particles to cool down inside the exchanger.

Flow rate = 100 $\frac{\mu L}{min}$ Flow rate = 200 $\frac{\mu L}{min}$ Flow rate = 300 $\frac{\mu L}{min}$

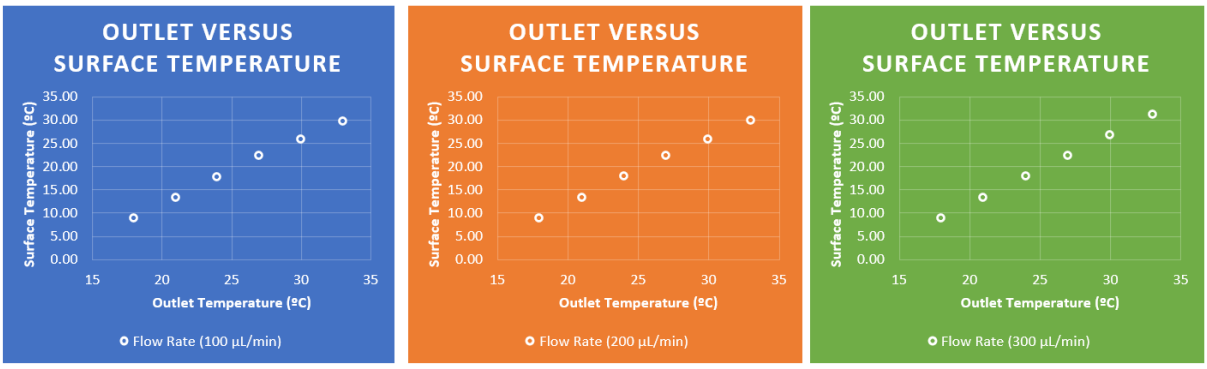


Figure 4.17. Simulated results

For research objectives, the heat exchanger's thermal performance had to be evaluated as well. Under the same experimental conditions, Figure 4.18 depicts the temperature distribution of the micro heat exchanger at various flow rates.

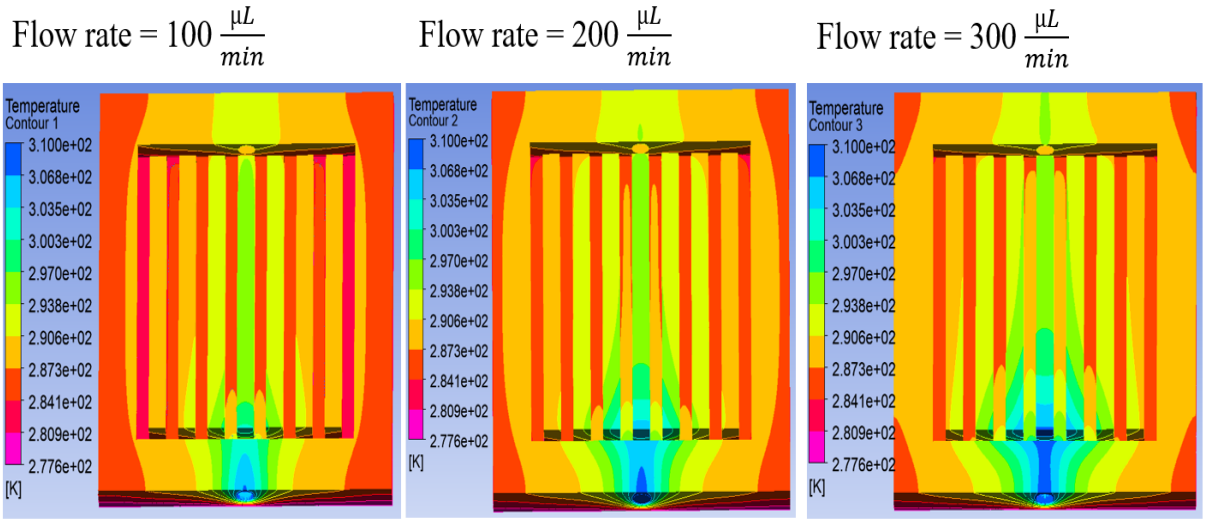


Figure 4.18. Temperature distribution results

By measuring the surface and fluid temperature of the heat exchanger at precise points, the theoretical findings were compared to the experimental results. To maintain the desired exit temperature, the surface temperature lowers with time. As the outflow temperature rises, so does the surface temperature. The surface temperature fluctuates more as the flow rate increases. The simulated and experimental findings were quite similar for the surface and outflow temperatures.

The tiny heat exchanger concept uses aggressive design limitations to transfer a higher rate of heat transfer/frontal area while preserving its rate of heat transfer/volume and mass advantage. These findings point to ideal conditions for future animal and human experimentation. The micro model of a U-type heat exchanger will help researchers better comprehend complex flow patterns in 3D and pave the way for novel ways to treat brain injuries in people and animals with small form factors.

# Chapter 5. Future Directions

Our model's development will aid surgeons in more precisely cooling the brain based on the input parameters for each patient. As a result, the operation will be safer, and the negative repercussions of using poor approaches will be reduced. It has been discovered that thorough system tuning is required to utilize active brain cooling fully. Different system factors may play a role in achieving the best solution, depending on the application goal. As a result, automatic multi-objective optimization approaches are recommended. One way to improve heat transfer is to use microstructure heat exchangers. The current research focuses on the effects of microstructure heat exchanger enhancement, explicitly using a fin arrangement. Apart from the impact of increased heat transfer rates of fin geometry in the microstructure heat exchanger, the study demonstrates that different flow rates, which are linked to heat transfer, have a significant impact on overall heat exchanger efficiency. This tendency of rising heat transfer efficiency with increasing flow rate is expected, but it is especially noticeable in the microstructure heat exchanger studied here.

The miniature heat exchanger was successfully manufactured within modest design restrictions. Because the heat exchanger is made utilizing the 3D printing process, alignment, and bonding, using a material with better thermal properties can improve the heat exchanger's thermal performance. Fabrication methods such as ceramic moulding and metal injection moulding should be investigated since they could be an economical and quick way to produce high-performance micro heat exchangers. Electroplating nickel on a thinner electroless plated layer should be examined to minimize the cost of the micro heat exchanger because electroplating solutions are about an order of magnitude less expensive than electroless plating solutions. After the backing has been removed, methods of cleaning the moulded bits of plastic should be researched, and subsequent manufacturing stages (sputtering and electroless plating) should be undertaken in a cleanroom environment to eliminate faults that cause leakage.

## 5.1. Micro-Heat Exchanger Strength Testing

The ratio of heat transmitted in the actual heat exchanger to the heat transferred in the ideal heat exchanger is defined as heat exchanger efficiency. Modelling is used to determine ideal performance, which takes into account constraints such as the second law of thermodynamics, which states that increasing amounts of energy are squandered every time it is transported or converted. The levels involved in achieving 'perfect' or 'ideal' heat exchanger efficiency, which transmits the most heat while producing the least entropy, serve as a baseline against which the existing micro heat exchanger can be assessed [74]. Typically, heat exchanger performance is measured solely in terms of heat transfer rate, with operational efficiency being ignored. A heat exchanger's performance, on the other hand, can be examined with a limited number of measures. As the number of measurements grows, so does the number of available analysis methods. This information can be used to justify raising the number of measurements in specific locations. Performance monitoring can also be applied to other processes, allowing for tracking larger entities by combining the results of multiple operations.

The fluid's thermal conductivity and convective heat transfer coefficient determine the heat exchanger's efficiency. The thermal conductivity, density, specific heat, and viscosity of fluids affect the convective heat transfer coefficient. The opening temperature of the heat exchanger, the rate of fluid filling, the physical nature of the liquid, the working temperature of the tube, angle, tube spacing, tube length, hot and cold fluid flow, and surrounding conditions all affect heat transfer performance of micro heat exchangers [75]. The performance of the micro heat exchanger might be measured using a testing instrument. The testing technique could include flow meters, pressure transducers, pressure gauges, and thermocouples. The fluid's intake and exit temperatures, pressure decreases, and flow rates should be measured.

An uncertainty analysis could be used to measure the testing results' accuracy and data validity.

5.2. Trial on Animals

Micro heat exchangers connected to the brain's lateral ventricles can successfully cool the CSF, lowering brain temperature while preserving systemic normothermia. The heat exchanger system circulates the cold fluid, which cools the CSF in the brain. By conduction, the CSF cools the surrounding brain. In animal models, several researchers have demonstrated localized brain cooling to moderate hypothermic levels. The animal study might benefit from using the micro heat exchanger for CSF cooling simultaneously. When used with adequate counter-warming, a heat exchanger can successfully induce and sustain exclusive cerebral cooling [76]. Entire brain cooling could be safe, with no local or systemic side effects, and maybe desirable in specific animal populations.

Implementing this innovative CSF-based cooling platform will result in significant and uniform cooling across an animal's cortex, which has ventricular geography comparable to that of the human brain [77]. Surprisingly, the approach can chill both brain hemispheres with just one micro heat exchanger. Because the brain can be cooled selectively, avoiding the adverse side effects of whole-body cooling, CSF-based cooling provides a particularly efficient way for producing therapeutic hypothermia, increasing hope for improved clinical management of TBI or ischemia.

5.3. Trial on Humans

The heat exchanger could influence thermal transfer and help maintain or cool the brain by circulating cerebrospinal fluid flow around the brain. Evaporation at the sinus surface produces a cooling effect conveyed to the cisterns, dispersing heat from the CSF that has been absorbed from the brain parenchyma [78]. According to various research, having chilled

CSF around the brain provides mild cooling with a medium cooling potential. The heat exchanger can be used in more studies on human brains to discover its success.

## References


1. Alam, Tanjebul; Bacellar, Daniel; Ling, Jiazhen; and Aute, Vikrant. *Numerical Study And Validation Of Melting And Solidification In PCM Embedded Heat Exchangers With Straight Tube*. International Refrigeration and Air Conditioning Conference. Paper 2259.

2. Al-Asadi, Mushtaq T., et al. *Heat transfer enhancement in a micro-channel cooling system using cylindrical vortex generators*. International Communications in Heat and Mass Transfer 74 (2016): 40-47.

3. Arani AAA, Akbari OA, Safaei MR, Marzban A, Alrashed AA, Ahmadi GR, Nguyen TK. *Heat transfer improvement of water/single-wall carbon nanotubes (SWCNT) nanofluid in a novel design of a truncated double-layered microchannel heat sink*. Int J Heat Mass Transf 113:780-795.

4. Ayub, Zahid H. *Plate Heat Exchanger Literature Survey and New Heat Transfer and Pressure Drop Correlations for Refrigerant Evaporators*. Heat Transfer Engineering. 24 (2003): p. 16-23.

5. Bahmani MH, Sheikhzadeh G, Zarringhalam M, Akbari OA, Alrashed AA, Shabani GAS, Goodarzi M. *Investigation of turbulent heat transfer and nanofluid flow in a double pipe heat exchanger*. Adv Powder Technol 29:273-282.

6. Bahrami, Arash & Haghighi Poshtiri, Amin & Mirzazade, Ali. *Nusselt Number Correlations for Forced Convection in a Microchannel Including Discrete Heat Sources*. Journal of Thermophysics and Heat Transfer. Vol. 34. P. 1-12.

7. Bayendang, Nganyang & Kahn, Mohamed-Tariq & Balyan, V. & Draganov, Ivo & Pasupathi, Sivakumar. *A Comprehensive Thermoelectric Cooler (TEC) Modelling*. SSRN Electronic Journal. 10.2139/ssrn.3735378.

8. Bistafa, Sylvio R. *On the development of the Navier-Stokes equation by Navier*. Revista Brasileira De Ensino De Fisica, 40 (2017): n. pag.

9. Brandner, Jürgen J et al. *METALLIC MICRO HEAT EXCHANGERS: PROPERTIES, APPLICATIONS AND LONG TERM STABILITY*.

10. Brinker T, Stopa E, Morrison J, Klinge P. *A new look at cerebrospinal fluid circulation.* Fluids Barriers CNS. 2014;11:10.

11. Castren M, Nordberg P, Svensson L, Taccone F, Vincent JL, Desruelles D, Eichwede F, Mols P, Schwab T, Vergnion M., et al. *Intra-arrest transnasal evaporative cooling: a randomized, prehospital, multicenter study*. Pre-ROSC IntraNasal Cooling Effectiveness. 122(7):729-736.

12. Chabi A, Zarrinabadi S, Peyghambarzadeh S, Hashemabadi S, Salimi M. *Local convective heat transfer coefficient and friction factor of CuO/water nanofluid in a microchannel heat sink*. Heat Mass Transf 53:661-671.
13. Cheng H, Shi J, Zhang Q, Yin H, Wang L. *Epidural cooling for selective brain hypothermia in porcine model*. Acta Neurochir (Wien) 2006;148:559-564.

14. Cormac Eason, Tara Dalton, Mark Davies, Cian O'Mathúna & Orla Slattery. *Direct Comparison between Five Different Microchannels, Part 2: Experimental Description and Flow Friction Measurement*. Heat Transfer Engineering. 26:3, p. 89-98.

15. Cruz, Patricia & Yamat, Ed-Jefferson & Nuqui, Jesus Patrick & Soriano, Allan. *Computational Fluid Dynamics (CFD) Analysis of the Heat Transfer and Fluid Flow of Copper (II) Oxide-Water Nanofluid in a Shell and Tube Heat Exchanger*. Digital Chemical Engineering. 100014.

16. Cui G., Liu Y., Gao G., Liu H., Kou Z. *Microstructure and High-Temperature Wear Performance of FeCr Matrix Self-Lubricating Composites from Room Temperature to 800 °C*. Materials (Basel). 2019 Dec 20;13(1):51.

17. Dang, Thanhtrung & Jyh-tong, Teng & Jiann-cherng, Chu. *Effect of Flow Arrangement on the Heat Transfer Behaviors of a Microchannel Heat Exchanger*. Lecture Notes in Engineering and Computer Science. 2182.

18. Davson H. *Physiology of the cerebrospinal fluid*. Churchill; London: 1967.

19. Deng, Y., Menon, S., Lavrich, Z., Wang, H., and Hagen, C. L. *Design, simulation, and testing of a novel micro-channel heat exchanger for natural gas cooling in automotive applications*. United States: N. p., 2017. Web.

20. Dohi K, Jimbo H, Abe T, Aruga T. *Positive selective brain cooling method: a novel, simple, and selective nasopharyngeal brain cooling method*. Acta Neurochirurg Suppl. 2006;96:409-12.

21. Eide, Per & Mardal, Kent-Andre & Lindstrøm, Erika & Ringstad, Geir. *Cerebrospinal Fluid Volumetric Net Flow Rate and Direction in Idiopathic Normal Pressure Hydrocephalus*. SSRN Electronic Journal. 10.2139/ssrn.3242820.

22. Ezhilana, M. et al. *EXPERIMENTAL AND CFD SIMULATION ANALYSIS OF MICRO CHANNEL HEAT EXCHANGER TO IMPROVE THE PRESSURE DROP AND HEAT TRANSFER CHARACTERISTICS USING R 410 A*. (2016).

23. Fazel Bakhsheshi M, Keenliside L, Lee TY. *A novel selective cooling system for the brain: feasibility study in rabbits vs piglets*. Intensive Care Med Exp, 2018. Nov 1;6(1):45.

24. Fedorov, A.G. and Viskanta, R. *Three-dimensional conjugate heat transfer in the microchannel heat sink for electronic packaging*. International Journal of Heat and Mass Transfer, Vol. 43, pp. 399-415.

25. Gard A, Tegner Y, Bakhsheshi MF, Marklund N. *Selective head-neck cooling after concussion shortens return-to-play in ice hockey players*. Concussion. 2021 Apr 15;6(2):CNC90.

26. Ghani I.A., Sidik N.A.C., Mamat R., Najafi G., Ken T.L., Asako Y., Japar W.M.A.A. *Heat transfer enhancement in microchannel heat sink using hybrid technique of ribs and secondary channels*. Int. J. Heat Mass Transf. 2017;114:640-655.

27. Giustini A, Pistarini C, Pisoni C. *Traumatic and nontraumatic brain injury*. Handb Clin Neurol. 2013;110:401-9.

28. Guo Z Y. *Characteristics of microscale fluid flow and heat transfer MEMS*. Proceeding of the international conference on Heat and Transport phenomena in microscale, Banff Canada, 2004:24-31.

29. Harris B, Andrews PJD, Murray GD., et al. *Systematic Review of Head Cooling in Adults After Traumatic Brain Injury and Stroke*. Southampton (UK): NIHR Journals Library; 2012 Nov. (Health Technology Assessment, No. 16.45.) Appendix 7, Non-invasive head-cooling methods and devices.

30. Hayashi, Y, Saneie, N, Kim, YJ, & Kim, J. *Thermal Performance and Pressure Drop of Galinstan-Based Microchannel Heat-Sink for High Heat-Flux Thermal Management*. Proceedings of the ASME 2015 13th International Conference on Nanochannels, Microchannels, and Minichannels collocated with the ASME 2015 International Technical Conference and Exhibition on Packaging and Integration of Electronic and Photonic Microsystems. ASME 2015 13th International Conference on Nanochannels, Microchannels, and Minichannels. San Francisco, California, USA. July 6-9, 2015. V001T07A012.

31. Heresztyn, AJH, & DeJong Okamoto, NC. Thermal Design of Microchannel Heat Sinks for Low-Orbit Micro-Satellites. *Proceedings of the ASME 3rd International Conference on Microchannels and Minichannels*. *ASME 3rd International Conference on Microchannels and Minichannels, Part B cont'd*. Toronto, Ontario, Canada. June 13-15, 2005. pp. 159-165.

32. Hoedemaekers CC, Ezzahti MM, Gerritsen AA, van der Hoeven JG. *Comparison of different cooling methods to induce and maintain normo-and hypothermia in ICU patients: a prospective intervention study*. Crit Care. 2007;2411:R91.

33. Hou G.L., An Y.L., Zhao X.Q., Zhou H.D. *Chen J.M. Effect of alumina dispersion on oxidation behavior as well as friction and wear behavior of HVOF-sprayed CoCrAlYTaCSi coating at elevated temperature up to 1000 °C*. Acta Mater. 2015;95:164-175.

34. Howden L, Giddings D, Power H, Aroussi A, Vloeberghs M, Garnett M, Walker D. *Three-dimensional cerebrospinal fluid flow within the human ventricular system*. Comput Methods Biomech Biomed Engin. 2008 Apr;11(2):123-133.

35. Hyder AA, Wunderlich CA, Puvanachandra P, Gururaj G, Kobusingye OC. *The impact of traumatic brain injuries: a global perspective*. NeuroRehabilitation. 2007;22(5):341-353.

36. Idris, Zamzuri, et al. *Direct Brain Cooling in Treating Severe Traumatic Head Injury*. Traumatic Brain Injury - Neurobiology, Diagnosis and Treatment, edited by Yongxia Zhou, IntechOpen, 2019. 10.5772/intechopen.84685.

37. Iliff JJ., et al. *A paravascular pathway facilitates CSF flow through the brain parenchyma and the clearance of interstitial solutes, including amyloid*. Science Translational Medicine, 2012. 4(147): 147ra111.

38. Jang S. P., Choi S. U. *Cooling Performance of a Microchannel Heat Sink with Nanofluids*. Applied Thermal Engineering. Vol. 26, Nos. 17-18, 2006, pp. 2457-2463.

39. Japar, Wan Mohd. Arif Aziz, Sidik, Nor Azwadi Che, Saidur, Rahman, Asako, Yutaka and Nurul Akmal Yusof, Siti. *A review of passive methods in microchannel heat sink application through advanced geometric structure and nanofluids: Current advancements and challenges*. Nanotechnology Reviews, vol. 9, no. 1, 2020, pp. 1192-1216.

40. Jassam YN, Izzy S, Whalen M, McGavern DB, El Khoury J. *Neuroimmunology of traumatic brain injury: time for a paradigm shift*. Neuron. 2017;95(6):1246-1265.

41. Johanson C, Stopa E, McMillan P, Roth D, Funk J, Krinke G. *The distributional nexus of choroid plexus to cerebrospinal fluid, ependyma and brain: toxicologic/pathologic phenomena, periventricular destabilization, and lesion spread*. Toxicol Pathol. 2011;39:186-212.

42. Kallmunzer B, Koehn J, Abrar D, Schwab S, Kollmar R. *First experiences with the new EMCOOLS device for selective neck-cooling for patients with acute ischemic stroke*; 4th International Hypothermia Symposium; Tokyo, Japan. September 2011.

43. Kandlikar, S. G. *Microchannels: Rapid Growth of a Nascent Technology*. ASME. J. Heat Transfer. April 2010; 132(4): 040301.

44. Kandlikar, SG. *Microchannels and Minichannels: History, Terminology, Classification and Current Research Needs.* Proceedings of the ASME 2003 1st International Conference on Microchannels and Minichannels. 1st International Conference on Microchannels and Minichannels. Rochester, New York, USA. April 24-25, 2003. pp. 1-6.

45. King C, Robinson T, Dixon CE, Rao GR, Larnard DJ, Nemoto EM. *Brain temperature profiles during epidural cooling with the Chillerpad in a monkey model of traumatic brain injury*. J Neurotrauma 2010;27:1895-1903.

46. Lehtinen MK, Zappaterra MW, Chen X, Yang YJ, Hill AD, Lun M, Maynard T, Gonzalez D, Kim S, Ye P, D'Ercole AJ, Wong ET, LaMantia AS, Walsh CA. *The cerebrospinal fluid provides a proliferative niche for neural progenitor cells*. Neuron. 2011;69:893-905.

47. Li Z X,Wang W, Guo Z Y. *Effects of axial heat conduction in wall on convection inmicrotubes.Conf.on Microchannels and Minichannels*, April24-25,2003,Rochester,New York,USA, 2003:327-333.

48. Maleki H, Safaei MR, Togun H, Dahari M. *Heat transfer and fluid flow of pseudo-plastic nanofluid over a moving permeable plate with viscous dissipation and heat absorption/generation*. J Therm Anal Calorim 2018:1-12.

49. McCormack, Matthew & Fang, Fengzhou & Zhang, Jufan. *Numerical Analysis of Microchannels Designed for Heat Sinks*. Nanomanufacturing and Metrology. 10.1007/s41871-021-00118-2.

50. Mehendale, Sunil & Jacobi, A. & Shah, R. *Fluid Flow and Heat Transfer at Micro and Meso-Scales With Application to Heat Exchanger Design*. Applied Mechanics Reviews. 53. 10.1115/1.3097347.

51. Mestre, H., Tithof, J., Du, T. et al. *Flow of cerebrospinal fluid is driven by arterial pulsations and is reduced in hypertension*. Nat Commun 9, 4878 (2018).

52. Moomiaie RM, Gould G, Solomon D, Simmons J, Kim J, Botta D, Elefteriades JA. *Novel intracranial brain cooling catheter to mitigate brain injuries*. J Neurointerv Surg. 2012 Mar;4(2):130-3.

53. Moomiaie RM, Gould G, Solomon D et al. *Novel intracranial brain cooling catheter to mitigate brain injuries*. Journal of NeuroInterventional Surgery 2012;**4:**130-133.

54. Mooney MR, Unger BT, Boland LL., et al. *Therapeutic hypothermia after out-of-hospital cardiac arrest: evaluation of a regional system to increase access to cooling*. Circulation. 2011;124(2):206-214.

55. Moore EM, Nichol AD, Bernard SA, Bellomo R. *Therapeutic hypothermia: benefits, mechanisms and potential clinical applications in neurological, cardiac and kidney injury*. Injury. 42(9):843-854.

56. Nikkhah, V., Nakhjavani, S. *Thermal performance of a micro heat exchanger (MHE) working with zirconia-based nanofluids for industrial cooling*. Int J Ind Chem 10, 193-204 (2019).

57. Panda, Kanishka & Hirokawa, Tomoki & Huang, Long. *Design Study of Microchannel Heat Exchanger Headers Using Experimentally Validated Multiphase Flow CFD Simulation*. Applied Thermal Engineering. p. 178-183.

58. Pittl U, Schratter A, Desch S, Diosteanu R, Lehmann D, Demmin K, Hörig J, Schuler G, Klemm T, Mende M, Thiele H. *Invasive versus non-invasive cooling after in- and out-of-hospital cardiac arrest: a randomized trial*. Clin Res Cardiol. 2013 Aug;102(8):607-14.

59. Ryu, J.H., Choi, D.H. and Kim, S.J. *Numerical optimization of the thermal performance of a microchannel heat sink*. International Journal of Heat and Mass Transfer, Vol. 45, pp. 2823-2827.

60. S. M. Joshi and S. R. Anand. *Design of conical helical coil heat exchanger for waste heat recovery system*. International Conference on Technologies for Sustainable Development (ICTSD), 2015, pp. 1-8.

61. Sarafraz M, Arya H, Saeedi M, Ahmadi D. *Flow boiling heat transfer to MgO-therminol 66 heat transfer fluid: experimental assessment and correlation development*. Appl Therm Eng 138:552-562.

62. Scotti, Gianmario & Franssila, Sami. *A micro heat exchanger microfabricated from bulk aluminium*. Journal of Physics: Conference Series. 557. 012069.

63. Singhal, V, Liu, D, & Garimella, SV. Analysis of Pumping Requirements for Microchannel Cooling Systems. *Proceedings of the ASME 2003 International Electronic Packaging Technical Conference and Exhibition. 2003 International Electronic Packaging Technical Conference and Exhibition, Volume 2*. Maui, Hawaii, USA. July 6-11, 2003. pp. 473-479.

64. Smith KD, Zhu L. *Brain hypothermia induced by cold spinal fluid using a torso cooling pad: theoretical analyses*. Med Biol Eng Comput. 2010 Aug;48(8):783-91.

65. Steinke, ME, & Kandlikar, SG. *Single-Phase Liquid Heat Transfer in Microchannels*. Proceedings of the ASME 3rd International Conference on Microchannels and Minichannels. ASME 3rd International Conference on Microchannels and Minichannels, Part B cont'd. Toronto, Ontario, Canada. June 13-15, 2005. pp. 667-678.

66. T. Bello-Ochende, F. Ighalo and J. Meyer. *Mathematical Optimization: Application to the Design of Optimal Micro-channel Heat Sinks in Computational Modeling*. Southern Conference on, Rio Grande, Brazil, 2009 pp. 1-6.

67. Trp, Anica. *An experimental and numerical investigation of heat transfer during technical grade paraffin melting and solidification in a shell-and-tube latent thermal energy storage unit*. Solar Energy 79 (2005): pp. 648-660.

68. Uruba, Vaclav. *Reynolds number in laminar flows and in turbulence*. AIP Conference Proceedings. 2118. 020003.

69. Ventola L., Dialameh M., Fasano M., Chiavazzo E., Asinari P. *Convective heat transfer enhancement by diamond shaped micro-protruded patterns for heat sinks: Thermal fluid dynamic investigation and novel optimization methodology*. Appl. Therm. Eng. 2016;93:1254-1263.

70. Vilarrubí M., Riera S., Ibañez M., Omri M., Laguna G., Frechette L., Barrau J. *Experimental and numerical study of micro-pin-fin heat sinks with variable density for increased temperature uniformity*. Int. J. Therm. Sci. 2018;132:424-434.

71. Walsh, John J et al. *Dynamic Thermal Mapping of Localized Therapeutic Hypothermia in the Brain*. Journal of neurotrauma vol. 37,1 (2020): pp. 55-65.

72. Wen D., Ding Y. *Experimental Investigation into Convective Heat Transfer of Nanofluids at the Entrance Region Under Laminar Flow Conditions*. International Journal of Heat and Mass Transfer, Vol. 47, No. 24, 2004, pp. 5181-5188.

73. Yousefi, Kianoosh and Alireza Razeghi. *Determination of the critical reynolds number for flow over symmetric NACA airfoils*. (2018).

74. Yu, Shimin, et al. *Effect of Prandtl Number on Mixed Convective Heat Transfer from a Porous Cylinder in the Steady Flow Regime*. Entropy, vol. 22, no. 2, Feb. 2020, p. 184.

75. Yunlong, Qiu, et al. *An Experimental Study of Microchannel and Micro-Pin-Fin Based On-Chip Cooling Systems with Silicon-to-Silicon Direct Bonding.* Sensors. 20(2020): 5533.

76. Z. Jie, R. Yan, Z. Lihong and L. Huimin. *Analysis of Influencing factors of heat transfer performance of heat pipe heat exchanger*. International Conference on Energy and Environment Technology, 2009, pp. 37-40.

77. Zhang, Rui et al. *Microstructure and Tribological Properties of Spark-Plasma-Sintered $Ti_3SiC_2$-Pb-Ag Composites at Elevated Temperatures*. Materials (Basel, Switzerland) vol. 15,4 1437.

78. Zhong Y., Zhou C., Chen S., Wang R.Y. *Effects of temperature and pressure on stress corrosion cracking behavior of 310S stainless steel in chloride solution*. Chin. J. Mech. Eng. 2016;30:200-206.

# Vita

Sachin Dahiya received his Bachelor of Technology in Mechanical Engineering from Maharishi Markandeshwar University, India, in 2019. After completing his bachelor's degree, he applied for graduate school and got admitted into the Louisiana State University graduate school for Mechanical Engineering. During his tenure at LSU, he worked as a Teaching Assistant in the School of Mechanical and Industrial Engineering's thermal systems lab. In August 2022, he will receive his Master of Science in Mechanical Engineering (MSME).